Atmos. Chem. Phys., 26, 5839–5860, 2026
https://doi.org/10.5194/acp-26-5839-2026

Atmospheric Chemistry and Physics
Open Access
EGU

Unprecedented radioactive pollution in Spitsbergen's air – first data of the 21st century

Anna Cwanek[1], Agnieszka Burakowska[2], Ewa Nalichowska[1], Magdalena Długosz-Lisiecka[3], Marek Kubicki[4], Tomasz Wawrzyniak[4], Edyta Łokas[1], Michał Gryziński[2], and Gabriela Lubera[1]

[1]Institute of Nuclear Physics, Polish Academy of Sciences, 31-342 Kraków, Poland
[2]National Centre for Nuclear Research, 05-400 Otwock-Świerk, Poland
[3]Lodz University of Technology, Institute of Applied Radiation Chemistry, 90-924 Łódz, Poland
[4]Institute of Geophysics, Polish Academy of Sciences, 01-452 Warszawa, Poland

Correspondence: Anna Cwanek (anna.cwanek@ifj.edu.pl)

Received: 3 April 2025 – Discussion started: 13 May 2025
Revised: 3 March 2026 – Accepted: 30 March 2026 – Published: 29 April 2026

Abstract. This study investigated the Arctic troposphere, providing a comprehensive experimental database on nuclear aerosols that has significantly improved since 1999. The activity concentrations of ^{238}Pu, $^{239+240}$Pu, and ^{241}Am were measured in surface air at Hornsund, Spitsbergen, from 2007–2021. A multivariate approach, incorporating meteorological data, gamma-emitter records, and isotopic ratios, was employed to explain the dynamics of change and the provenance of transuranium elements. Levels of ^{238}Pu and $^{239+240}$Pu were found comparable to those documented over the past decades at various locations. The highest activity concentrations were 6.61 nBq m^{-3} for ^{238}Pu and 15.5 nBq m^{-3} for $^{239+240}$Pu, observed in 2015. Although coinciding with the resuspension and atmospheric transport of radionuclides due to the 2015 wildfires near the Chernobyl zone, a direct contribution to Hornsund remains uncertain. Further data exploration revealed a correlation between $^{239+240}$Pu and seasonal processes, including local dust redistribution and horizontal tropospheric transport of haze layers from distant areas. While similar mechanisms likely regulated a portion of ^{238}Pu, its random enrichment relative to known nuclear events was frequently detected. As a general trend, ^{241}Am exhibited notably high activity concentrations, reaching up to 354 nBq m^{-3} in 2019. Episodic signals of ^{237}Np were identified in 2013, 2014, and 2018. All occurrences of ^{241}Am, ^{237}Np, and outliers of ^{238}Pu were not linked to natural processes; hence, the possibility of recent radioactive emissions should be considered. Trajectory simulations conducted for 2019 indicated prominent transport pathways to Hornsund from northern Eurasia.

1 Introduction

Advances in nuclear science during the 20th century have led to the systematic production of a novel form of environmental contamination on a global scale. Introduced radionuclides, commonly classified as artificial, technogenic, manmade, or anthropogenic, were previously non-existent or present only in ultra-trace quantities across the Earth system. Although the nuclear era continues today, it has undergone significant changes in scope, objectives, and main directions over time. The initial focus on military applications has since shifted towards the development of nuclear power plants, nuclear medicine, and all radioactive-materials-handling industries. Undoubtedly, this ongoing revolution has brought a plethora of benefits. However, the parallel identification of new radionuclide emissions and their transport over long distances from the epicentre – with the potential to increase natural background radiation levels – has heightened public awareness of the necessity to monitor and control the radiological situation routinely. These measures are required not only for critical groups, objects, or areas but also to review the exposure of the general population and the surrounding environment at large. Safety standards for radiological protection, established by organisations such as the International Atomic Energy Agency (IAEA), the Commission of

the European Communities (CEC), and the Organisation for Economic Co-operation and Development/Nuclear Energy Agency (OECD/NEA), are based on conceptual frameworks proposed by the International Commission on Radiological Protection (ICRP) (Engelbrecht and Schwaiger, 2008; ICRP, 1991, 2007). Monitoring air radioactivity appears particularly important, given that inhalation represents a major exposure pathway.

The injection of anthropogenic radionuclides (^{54}Mn, ^{55}Fe, ^{89,90}Sr, ^{95}Zr, ^{103,106}Ru, ^{125}Sb, ^{131}I, ^{133,135}Xe, ^{134,135,137}Cs, ^{141,144}Ce, ^{236}U, ^{237}Np, ^{238,239,240,241}Pu, ^{241}Am, ^{242,243,244}Cm, etc.) into the total environment has been the consequence of a variety of specific events (UNSCEAR, 1982, 2000a), as outlined below:

a. nuclear explosions and safety tests (> 2300):
   - 543 atmospheric nuclear weapon tests (1945–1980) with a legacy of global fallout (GF),
   - underwater/underground nuclear weapon tests,
   - sub-critical safety trials to burn or explode U and/or Pu without a fission yield,

b. releases from nuclear reprocessing plants (NRP) and plutonium production plants (PPP), e.g., Sellafield, Cap de la Hague, Mayak, Tomsk,

c. nuclear reactor accidents in nuclear power plants (NPP), e.g., Chernobyl, Fukushima,

d. satellite, aircraft and submarine accidents, e.g., SNAP 9A, Cosmos 954, Thule, Komsomolets K-278,

e. effluents associated with radionuclide production for scientific and medical applications,

f. leaching from dumped nuclear material,

g. U-mining and tailing,

h. conventional explosions, including depleted uranium (DU) weapons.

Radioactive debris, once released into the atmosphere, rapidly attaches to ambient aerosols and is subject to the mechanisms that govern air circulation. At least four factors must be given consideration when studying nuclear aerosol transport and deposition. Firstly, cooled debris halted within the stratosphere is distributed across broad layers and over a wide range of latitudes by eddy diffusion (Feely et al., 1989; UNSCEAR, 1982). Their subsequent descent into the upper troposphere is most common at middle latitudes and proceeds most rapidly in the spring season (Feely et al., 1989). The mean residence time of nuclear particles reaching the stratosphere has been estimated at 1.5±0.5 years (Hirose and Povinec, 2015). Secondly, the reduced stability of the troposphere during warmer months enhances the rate of vertical transport from the upper to the middle and lower troposphere (Aegerter et al., 1966). Solar heating triggers convective circulation, lifting surface air upward and drawing air from higher layers downward. This is especially prominent at middle latitudes. In polar regions, atmospheric stability inhibits vertical movement even during warmer months (Aegerter et al., 1966). The third factor involves the horizontal advection of lower-tropospheric air masses from middle to high latitudes, which peaks during the late winter season. Haze layers arriving in the Arctic are believed to originate from pollutants emitted in the middle-latitude regions of Asia, Europe and potentially North America (Rahn, 1981). The rate of haze particle delivery has been attributed to a combination of annual fluctuations in the transport regime and changes in pollutant removal (Barrie et al., 1981). The fourth process affecting temporal trends in airborne radioactivity is aerosol washout, particularly at sites with large seasonal variations in rainfall amount and frequency (Feely et al., 1989).

It is believed that no significant quantities of artificial radionuclides remain in the stratosphere, as the majority of contaminants derived from past atmospheric emissions – primarily attributable to nuclear weapons testing – have already descended (Hirose et al., 2003; Kierepko et al., 2016). The resuspension phenomenon, a secondary source of contamination, is considered the dominant mechanism for sustaining residual anthropogenic radioactivity near the surface of the Earth (Hirose and Povinec, 2015). Atmospheric resuspension arises from processes such as wind erosion of soil particles, sea spray, flying ash from biomass burning, or global desert dust events (Masson et al., 2010, 2021). Volcanic eruptions have additionally been hypothesised to enhance the transfer of anthropogenic radionuclides from the stratosphere to the troposphere (Alvarado et al., 2014). On the other hand, the recent worldwide releases of ^{131}I and ^{134,137}Cs from the Fukushima Daiichi Nuclear Power Plant (FDNPP) accident in 2011 (Koo et al., 2014; Povinec et al., 2013), alongside a 2017 episode of ^{106}Ru in the air over Europe (Bossew et al., 2019), serve as evidence that nuclear incidents can still occur. Continuous measurements of activity concentrations in the atmosphere provide one of the best means of identifying and differentiating between resuspended and freshly released radioisotopes. Moreover, the network of air monitoring stations, when used in conjunction with modelling tools, enables tracking of radioactive plume back to the point of discharge.

Investigations into nuclear aerosols commenced in the late 1950s and early 1960s. Air radioactivity sampling may serve one or more of the following purposes: (a) worker health protection to ensure exposures are within acceptable limits and As Low As Reasonably Achievable (ALARA); (b) environmental monitoring to ensure emissions of contaminants are within acceptable limits and ALARA; (c) process quality assurance and control to verify if all procedures function properly; and (d) emergency preparedness and response to provide a basis for appropriate action when an incident occurs (Hoover and Maiello, 2010). One of the most exten-

sive and detailed records on atmospheric radioactivity globally – the Surface Air Sampling Program (SASP) – was conducted by the Environmental Measurements Laboratory (EML) between 1963 and 1999 (Larsen et al., 1995), continuing the work initiated by the Naval Research Laboratory (NRL) during 1957–1962 (U.S. Atomic Energy Commission, U.S. Energy Research and Development Administration, U.S. Department of Energy). SASP's primary objective was to determine the spatial and temporal distribution of specific natural and artificial gamma, beta, and alpha emitters (^{7}Be, ^{54}Mn, ^{55}Fe, ^{89,90}Sr, ^{95}Zr, ^{109}Cd, ^{137}Cs, ^{141,144}Ce, ^{210}Pb, $^{238,239+240}$Pu) in ground-level air at monitoring stations worldwide. In addition to radionuclides of GF origin, the EML programme detected and characterised a post-Chernobyl plume over North America in 1986 (Feely et al., 1988; Larsen et al., 1989), as well as minute quantities of fission products in Alaska after accidental releases from the Tomsk-7 nuclear complex in 1993 (Larsen, 1994). The implementation of SASP was not limited solely to routine monitoring but also contributed to several scientific observations and discoveries. Notably, the compiled database enhanced the trajectory modelling of natural and artificial aerosols through the atmosphere, revealed seasonal cycles of ^{7}Be concentrations in surface air (Feely et al., 1989), or demonstrated the linkage between a decrease in the production rate of cosmogenic radionuclides and an increase in solar activity (Larsen, 1993). Furthermore, the SASP database has been utilised to simulate the global distributions of ^{222}Rn and ^{210}Pb within the EML's three-dimensional transport model (Lee and Feichter, 1995).

Presently, the majority of countries possess nationwide air-monitoring capabilities and participate in internationally coordinated network systems (e.g., CTBTO or Ro5 networks) (Baré et al., 2023; Coyne et al., 2012; Furuno et al., 2024; Steinhauser et al., 2014). Such cooperation facilitates the acquisition of data essential for assessing the radiological situation across vast territories, including even remote Arctic (except for Greenland and the Faroe Islands) and Antarctic regions (AMAP, 2015; Gorzkiewicz et al., 2022). Early-detection stations for atmospheric contamination operate continuously, providing rapid information on selected natural (^{7}Be, ^{22}Na, ^{40}K, ^{210}Pb, etc.) and possible artificial (^{54}Mn, ^{60}Co, ^{95}Zr, ^{103,106}Ru, ^{125}Sb, ^{131}I, ^{133}Xe, ^{134,137}Cs, ^{141,144}Ce, ^{241}Am, etc.) radioisotopes by gamma spectrometry. Some laboratories also employ alpha spectrometry or mass spectrometry to determine ^{238,239,240}Pu and ^{241}Am (artificial actinides) in air filter samples. Typically, the latter assessment is carried out in the context of a specific nuclear incident, thus encompassing a relatively limited timeframe (Alvarado et al., 2014; Chamizo et al., 2010; Masson et al., 2010). Longer-term studies are also performed, but less frequently (Kierepko et al., 2016; Lujaniene et al., 2012; Nalichowska et al., 2023).

In certain regions, no air monitoring programmes dedicated to anthropogenic actinides have been conducted since 2000. This is especially evident for atmospheric radioactivity in the Arctic, where data on levels, isotopic signatures, or temporal variations of ^{238,239,240}Pu and ^{241}Am are lacking in the 21st century. For several reasons, research in this domain is of particular interest and importance. Artificial actinides have attained tracer status in investigations of atmospheric circulation or natural "feeder" mechanisms through which previously deposited contaminants are transferred back to the air (Alvarado et al., 2014; Hirose et al., 2003; Hirose and Povinec, 2015; Masson et al., 2010). ^{238,239,240}Pu and ^{241}Am are recognised among the most radiotoxic elements that may be directly inhaled with aerosols or accumulate in plants and animals. Also noteworthy are the relatively long half-lives of these radionuclides (^{238,239,240}Pu: $T_{1/2} =$ 87.7 years, 2.41×10^{4} years, 6.56×10^{3} years, respectively; ^{241}Am: $T_{1/2} = 432.6$ years), implying that such pollution will persist in the environment over multiple generations. In the context of potential terrorist attacks involving "dirty bomb", undeclared nuclear activity, and any intentional or unintentional releases from nuclear installations, the development of novel monitoring strategies seems imperative (Mietelski and Povinec, 2020). Specifically, the world's national and international nuclear safety monitoring networks should incorporate routine measurements of pure beta and alpha emitters in the atmosphere.

The research project outlined in this paper aimed to address limitations in database capabilities and to enhance understanding of the processes governing artificial actinides suspended in the ground-level air layers of Hornsund, SW Spitsbergen, between 2007 and 2021. The following key objectives were defined and subsequently achieved:

a. determination of activity concentrations of ^{238}Pu, $^{239+240}$Pu, and ^{241}Am,

b. evaluation of mutual correlations of ^{238}Pu, $^{239+240}$Pu, and ^{241}Am against ^{7}Be, ^{137}Cs, ^{210}Pb, suspended dust, and selected meteorological factors,

c. analysis of seasonality and long-term trends in time-series for ^{238}Pu, $^{239+240}$Pu, and ^{241}Am,

d. estimation of ^{238}Pu/$^{239+240}$Pu and ^{241}Am/$^{239+240}$Pu activity ratios,

e. modelling of air trajectories in the event of unusual nuclear signals being detected.

2 Materials and methods

2.1 Study area and sampling

Long-term observations of atmospheric radioactivity in the Arctic are a central component of the Arctic Monitoring and Assessment Programme (AMAP) (AMAP, 2002, 2009, 2015). The geographical locations of air filter stations across

the AMAP region, including Iceland, the Canadian Arctic, northern Finland, Sweden, and Norway, with the Svalbard archipelago, are mapped in Fig. 1b. To the best of our knowledge, no coordinates are publicly available for nuclear aerosol samplers placed within the Russian Arctic (AMAP, 2009, 2015). Consequently, these stations are not shown on the map.

Air monitoring of radioisotopes is carried out at the Stanisław Siedlecki Polish Polar Station (77°00′ N, 15°33′ E, 10 m above sea level), one of the few permanently operating units north of the Arctic Circle (Fig. 1b) (Burakowska et al., 2021). The Polish Polar Station, located 300 m from the shore of Isbjørnhamna Bay in the Hornsund fjord of SW Spitsbergen, Svalbard archipelago (Fig. 1a and c), was established during the International Geophysical Year in 1957. Over decades, the site has evolved into a modern interdisciplinary scientific platform conducting research projects to better understand the functioning of the Arctic environment and the changes it undergoes (Wawrzyniak and Osuch, 2020).

A high-performance air intake system for the AZA-1000 model was launched at Hornsund in 2002 to enable continuous operation at low temperatures (Fig. 1d) (Burakowska et al., 2021). Aerosols are captured on Petrianov FPP-15-1.5 filters – made of chlorinated polyvinyl chloride (CPVC) fibre – that offer a high retention capacity for particles at least 0.3 µm in diameter. The filter efficiency for aerosols with diameters between 0.3 and 1.25 µm at linear air velocities of 0.25–0.4 $m\,s^{-1}$ ranges from 96 % to 99 % (Kierepko et al., 2016; Nalichowska et al., 2023). The high airflow (ca. 450 $m^3\,h^{-1}$) ensures the collection of a representative portion of aerosols in a single air filter sampled over a week from about 50 000–100 000 m^3 of pumped air. This research scope extended from 2007–2021, including the 2011–2013 gap in data collection, during which a substantial number of weekly filters were not available.

2.2 Meteorological data

Since July 1978, systematic, continuous measurements and observations have been conducted at the Hornsund meteorological site (indexed by the international numbering system 01003; https://oscar.wmo.int/surface/, last access: 1 April 2026; in accordance with World Meteorological Organisation (WMO) standards (Wawrzyniak and Osuch, 2020). A detailed description of the measurements and instruments is provided in a collective work edited by Marsz and Styszyńska (2013), while selected information on meteorological variables and sensors is presented in Table S1 in the Supplement.

The Svalbard archipelago experiences the highest air temperatures at northern latitudes, and the observed climate changes are the most pronounced on Earth (IPCC, 2019). An analysis of the climatological dataset spanning 40 years (1978–2018) offers a comprehensive overview of the meteorological conditions in the Hornsund region (Wawrzyniak and Osuch, 2020). The mean annual air temperature reaches −3.7 °C. The coldest month is March, with a mean air temperature of −10.2 °C, and the warmest month is July, with a mean air temperature of 4.6 °C. The West Spitsbergen Current contributes to a relatively moist climate, as evidenced by an annual precipitation amount of 478 mm. However, the interior of Spitsbergen is much drier (at around 200 mm). Winds blowing from the east along the Hornsund fjord are prevailing, and the wind speed regime shows lower average values in summer months (minimum 4.0 $m\,s^{-1}$ in June) but higher average values in winter months (maximum 7.1 $m\,s^{-1}$ in February). Such variability results from extreme cyclone activity that often occurs during Arctic winters (Rinke et al., 2017). The polar night lasts 104 d (31 October–11 February), while the polar day extends for 117 d (24 April–18 August).

This assessment encompassed daily data on air temperature (°C), sum of precipitation (mm), atmospheric pressure (hPa), relative humidity (%), cloudiness (octa), visibility (marine scale), sunshine duration (h), wind speed ($m\,s^{-1}$), and wind direction (°), collected between 2007 and 2021. For most meteorological parameters, daily mean values were calculated from 3 hourly measurements (eight values per day, between 00:00 and 21:00 UTC). Precipitation was measured every 6 h (12:00, 18:00, 00:00, and 06:00 UTC of the next day), whereas the daily sum of total solar radiation from the Campbell–Stokes recorder was obtained at midnight (Wawrzyniak and Osuch, 2020). The wind rose, changes in mean air temperature, and the sum of precipitation, determined daily in Hornsund for 2007–2021, are depicted in Fig. 2a, b, and d.

2.3 Gamma spectrometry measurements

A series of weekly air filters was supplied from the Polish Polar Station in Hornsund, Svalbard archipelago, to the National Centre for Nuclear Research (NCBJ) in Świerk, Poland. Before measurement, each sample was desiccated using halogen infrared heaters (500 W, 220–230 V) to determine the dry mass of the collected dust. Following this, the suspended particulate matter concentration (SPM, $\mu g\,m^{-3}$) was estimated at weekly intervals (Fig. 2c). Lastly, all filters were compressed individually to a diameter of 4.5 cm and a thickness of ca. 5 mm. Gamma-ray spectra were measured using a Canberra set, comprising HPGe detectors placed inside low-background shielding chambers with 10 cm-thick lead walls. Detector efficiencies range from 35 %–45 %, and energy resolutions are 1.9–2.0 keV for 1.33 MeV photons from ^{60}Co. Spectrometer calibration was performed utilising a certified source with well-known radioisotope activities. Data acquisition was facilitated by the Genie-2000 software (Mirion Technologies). Correction factors were applied to all results to account for decay during sampling, decay from the end of sampling to the start of measurement, and decay during measurement. The self-absorption

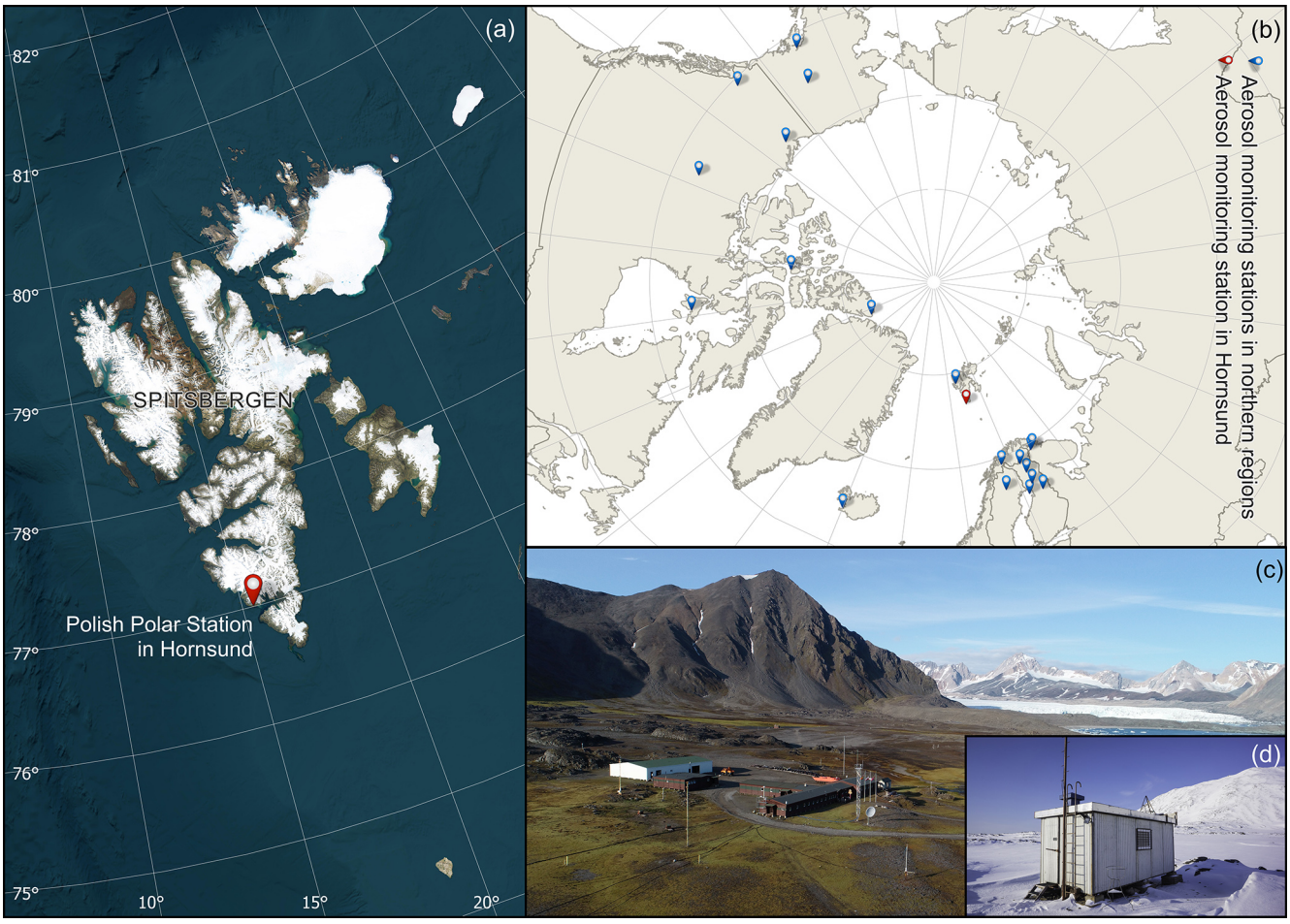

Figure 1. Map of Spitsbergen showing the location of the Stanisław Siedlecki Polish Polar Station in Hornsund **(a)**, the mapped sites for aerosol sampling in the northern regions **(b)**, the facilities of the Stanisław Siedlecki Polish Polar Station **(c)**, and the building housing the AZA-1000 air sampling system at the station **(d)**. The red pin marks the Stanisław Siedlecki Polish Polar Station, and the blue pins mark other stations. Basemap source: Esri, Maxar, Earthstar Geographics, and the GIS User Community | Powered by Esri. Photographs by T. Wawrzyniak.

correction proved negligible due to the samples' low height. The minimum detectable activity concentration for gamma spectrometry (MDC_γ, $\mu Bq\,m^{-3}$) was calculated according to the Currie law (Currie, 1968). Values of MDC_γ reached 0.1–10 $\mu Bq\,m^{-3}$, depending on the radionuclide. The present study incorporated weekly results on the volume activities (C, $\mu Bq\,m^{-3}$) of ^{7}Be, ^{137}Cs, and ^{210}Pb, arranged into a time series spanning 2007–2021.

2.4 Radiochemical procedures and alpha spectrometry measurements

The primary phase of the analysis determined the activity concentrations of ^{238}Pu, $^{239+240}Pu$, and ^{241}Am by alpha spectrometry. Considering the likely low quantities of artificial alpha emitters in the Hornsund atmosphere over the past 2 decades, it was hypothesised that the weekly aerosol sample would yield ^{238}Pu, $^{239+240}Pu$, and ^{241}Am levels below the minimum detectable activity concentrations for alpha spectrometry (MDC_α, $nBq\,m^{-3}$). A similar conclusion has been drawn by researchers investigating anthropogenic radioisotopes in the ground-level air of European cities during the 21st century (Kierepko et al., 2016; Lujaniene et al., 2012; Nalichowska et al., 2023). Therefore, weekly air filters from Hornsund were combined to represent approximately one-quarter of a year for the 2007–2010 and 2014–2021 intervals. Due to incomplete collection of weekly air filters from 2011–2013, only one biennial sample was prepared for 2011–2012, while two semi-annual samples were obtained in 2013. Typically, the aggregate samples consisted of 9–14 weekly air filters, with corresponding total air volumes ranging from 630 000–996 319 m^3.

The radiochemical separation of analytes from matrix components (such as organic matter, aeolian dust, anthropogenic particles, or filter material) followed the general procedure outlined by La Rosa and co-workers at the IAEA Lab-

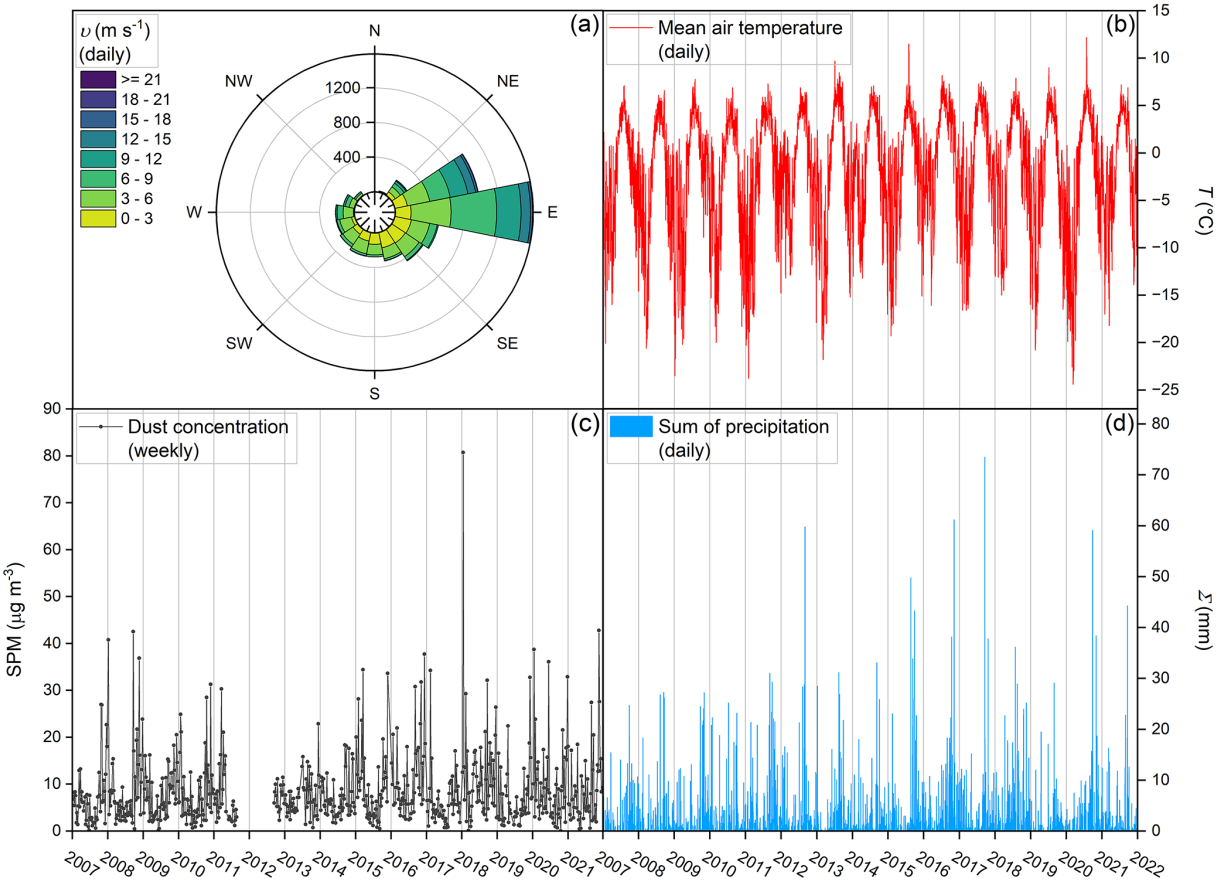

Figure 2. Wind rose according to wind speed (υ) and wind direction (N, NE, E, SE, S, SW, W, NW) **(a)**, together with the variability of mean air temperature (T) **(b)**, dust concentration (SPM) **(c)**, and sum of precipitation (Σ) **(d)**, all measured at Hornsund during 2007–2021.

oratories in Seibersdorf (La Rosa et al., 1992), as well as the method implemented at the Institute of Nuclear Physics, Polish Academy of Sciences (IFJ PAN) in Kraków (Mietelski et al., 2000, 2008). This approach had previously been tested in air filter investigations (Kierepko et al., 2016; Nalichowska et al., 2023). All non-concentrated reagents were prepared by dilution with ultrapure deionised water (Milli-Q®, 18.2 MΩ cm; Merck KGaA). The sample was initially incinerated at 600 °C in a muffle furnace. Next, internal tracers of ^{242}Pu (ca. 0.0041 Bq per sample) and ^{243}Am (ca. 0.0077 Bq per sample) were dosed (SRM 4334j and SRM 4332e, respectively; NIST). Near-complete sample mineralisation was achieved using concentrated acids (HF, HNO_3, HCl, and H_3BO_3), yielding a filtered 1 M HNO_3 solution. The plutonium fraction was separated from the 8 M HNO_3 feed solution via anion exchange chromatography with AmberChrom™ 1 × 8 resin (100–200 mesh; Sigma-Aldrich), preceded by adjustment of the Pu(IV) oxidation state. Given thorium's ability to adsorb onto the resin bed, its elution was performed prior to plutonium to prevent interference between plutonium and thorium isotopes during alpha-spectrum acquisition. Pu(IV) was washed out by passing through the column a mixture of 0.1 M HF–0.1 M HCl. The main effluent (8 M HNO_3) was expected to contain the americium analyte, significant quantities of lead, possible traces of thorium, rare-earth elements (REE), and other matrix impurities. Experience has shown that purification steps are necessary for effective isolation and measurement of the americium fraction. Removal of lead was achieved by retention on SR resin (100–150 µm particle size; Triskem International) from an 8 M HNO_3 solution. Alkali metals, alkaline earth metals, and anionic components were eliminated by subsequent precipitation of calcium oxalate at pH ∼ 2.5 and iron hydroxide(III) at pH ∼ 9. Repurification from any residual traces of thorium was then conducted using TEVA resin (100–150 µm particle size; Triskem International). The Am(III) was separated from the REE by anion-exchange chromatography on AmberChrom™ 1 × 8 resin (100–200 mesh; Sigma-Aldrich) in a methanol-acid medium. The isolated isotopes of Pu and Am were individually co-precipitated with NdF_3 from aqueous solutions and deposited onto Resolve® filters (0.1 µm pore size; Triskem International).

Separation of the interfering analytes, ^{237}Np and ^{242}Pu, from a few alpha sources proved essential for further assessment. Thus, a simplified version of the procedure by La Rosa et al. (2005) was employed. In the initial stage, the membrane filter was wet-digested with concentrated acids (H_3BO_3, HCl, $HClO_4$, and HNO_3). Next, plutonium and neptunium were adjusted to the required oxidation state (IV) and separated via column chromatography utilising an AmberChrom™ 1×8 resin (100–200 mesh; Sigma-Aldrich). The 8 M HNO_3 feed solution was passed through the column, resulting in strong retention of Np(IV) and Pu(IV). Traces of thorium were removed with a 10 M HCl solution, which additionally converted the column from nitrate to chloride form. Pu(III), reduced from Pu(IV), was selectively eluted using 0.1 M NH_4I–9 M HCl, whereas Np(IV) was washed out with a mixture of 0.1 M HF–0.1 M HCl. Finally, alpha sources of Pu and Np were individually re-prepared.

For data acquisition, alpha sources were positioned adjacent to passivated implanted planar silicon detectors (PIPS®, Mirion Technologies) inside the vacuum chambers of the AlphaAnalyst™ 7200 spectrometer (Mirion Technologies). The PIPS® detector, with a 450 mm^2 active area, has an efficiency of approximately 40 % and an energy resolution of 18 keV for 5.486 MeV alpha particles from ^{241}Am. All alpha spectra were processed in OriginPro® 2024b (OriginLab Corporation) using the Peak Analyser tools for baseline correction, peak detection, integration, or fitting. The latter option was applied to resolve overlapping spectral lines by fitting bigaussian curves. MDC_α values – calculated based on the Currie law (Currie, 1968) – typically varied from 0.01–0.1 nBq m^{-3} for $^{238,239+240}$Pu and ^{241}Am. The mean recoveries of Pu and Am fractions after chemical processing equalled 80.7 ± 2.5 % and 43.5 ± 2.2 %, respectively. The obtained dataset represented the activity concentrations (C, nBq m^{-3}) of $^{238,239+240}$Pu and ^{241}Am, largely determined in quarters between 2007 and 2021.

2.5 Statistical analysis and modelling

For each radioisotope except ^{237}Np, basic descriptive statistics were computed according to the time intervals at which the radioisotopes were measured. These included the minimum (min), 25th percentile ($Q1$), median, 75th percentile ($Q3$), maximum (max), interquartile range (IQR), mean, and standard deviation (SD). To spot outliers in the dataset, Tukey's interquartile range method with a multiplier $k = 3$ was employed (Hoaglin, 2003). Meteorological indicators, the SPM factor, and gamma emitters served as supporting variables to facilitate a comprehensive evaluation of the annual dynamics of artificial actinides in surface air. Consequently, the subsequent stages of statistical analysis involved converting daily and weekly data into quarterly formats. Data aggregation was performed using the following mathematical operations:

a. arithmetic mean for daily air temperature, atmospheric pressure, visibility, relative humidity, and cloudiness,

b. sum for daily precipitation and sunshine duration,

c. magnitude of the resultant wind velocity vector for each of the eight sectors (W, E, N, S, NW, NE, SE, SW), based on daily wind direction and speed,

d. sum of weekly activities or masses divided by the associated volume of pumped air in a specific quarter for gamma emitters and SPM, respectively.

The input database for calculating Spearman's correlation coefficient (R) was constructed by eliminating outliers in radioisotope activity concentrations. Given the non-quarterly format of the data, the 2011–2013 interval was omitted from the correlation matrix for alpha emitters against all other variables. The correlation was considered statistically significant at a probability level of less than or equal to 0.05 ($p \leq 0.05$). Data analysis and visualisation were performed in Python using the following libraries: NumPy, pandas, matplotlib, SciPy and seaborn.

For tracking aerosol fate dispersion, three-dimensional airmass trajectories were simulated using the Hybrid Single-Particle Lagrangian Integrated Trajectory (HYSPLIT) model developed by the National Oceanic and Atmospheric Administration (NOAA, U.S. Department of Commerce). The system has various applications in the domain of propagation and dispersion modelling of forest smoke, hazardous materials, chemicals, and radioactive substances, whether in gaseous or particulate form, including radionuclide decay (Stein et al., 2015). Backward simulations were performed for a final location at 77°00′ N, 15°33′ E (Hornsund), whereas a forward trajectory was generated from an initial location at 72°55′ N, 54°01′ E (Novaya Zemlya). All trajectories were reconstructed using archived meteorological data from the Climate Data Centre (CDC) and the Global Data Assimilation System (GDAS) repositories, both accessed via the NOAA Air Resources Laboratory (ARL) server.

3 Results and discussion

3.1 Descriptive statistics and time series

This study examined radioisotopes divided into two categories, here referred to as "target" and "background". The first group consisted of subject analytes (^{238}Pu, $^{239+240}$Pu, ^{241}Am), whereas the second group, mostly reported by Burakowska et al. (2021), provided supplementary information (^{7}Be, ^{137}Cs, ^{210}Pb). Table 1 summarises the descriptive statistics for both groups. As expected, naturally occurring radionuclides (^{7}Be, ^{210}Pb) in the lower atmosphere of Hornsund reached higher activity concentrations than the artificial ones (^{137}Cs, ^{238}Pu, $^{239+240}$Pu, ^{241}Am). The mean and

median values exhibited significant dispersion for each radionuclide, reflected by elevated standard deviations and interquartile ranges (Table 1). Estimating upper limits for outliers ($> Q3 + 3 \times \mathrm{IQR}$) was a pivotal phase in the assessment. All outlier points were highlighted in the time-series graphs (Figs. 3 and 4) and treated as potential radiological episodes. The outcomes were further displayed as combined violin and scatter plots, demonstrating non-normal distributions for ^{7}Be, ^{137}Cs, ^{210}Pb, ^{238}Pu, $^{239+240}$Pu and ^{241}Am (Fig. 5).

3.1.1 Background radioisotopes

Cosmogenic ^{7}Be ($T_{1/2} = 53.22$ d) is produced through the spallation of light atomic nuclei (such as carbon, nitrogen, and oxygen) by primary (protons) and secondary (neutrons) particles of cosmic radiation (Beer et al., 2019). Gäggeler (1995) reported that approximately 67 % of ^{7}Be forms in the stratosphere, with the remaining 33 % in the troposphere. ^{7}Be maxima are regularly observed in late spring (2nd/3rd quarter) in ground-level air layers at mid-latitudes, coinciding with intensive exchange between the stratosphere and the upper troposphere, followed by vertical transport within the middle and lower troposphere (Błażej and Mietelski, 2014; Dueñas et al., 2001; Grossi et al., 2016; Kulan et al., 2006). In contrast, atmospheric investigations at Hornsund station (Burakowska et al., 2021) revealed ^{7}Be activity concentration peaks in the late winter (1st/2nd quarter), as depicted in Fig. 3. Reduced vertical mixing of air masses in polar regions leads to lower ^{7}Be levels in the 2nd/3rd quarter compared with temperate zones. Therefore, the seasonal fluctuations of ^{7}Be in Hornsund are considered mainly governed by the horizontal tropospheric transfer of haze layers from Eurasian regions that reach higher latitudes during late winter months. Another process involved is wet scavenging, in which aerosols are washed out of the atmosphere and deposited onto Earth's surface. Long-term data analysis also confirmed the connection between the ^{7}Be air concentration and the 11-year solar activity cycle. The intensity of cosmic radiation has been shown to decrease with increasing solar activity (Beer et al., 2019). Hence, the atmospheric production of ^{7}Be is inversely proportional to the sunspot number. Between 2002 and 2017, as explored by Burakowska et al. (2021), the lower sunspot numbers per week occurred in 2008–2010, which likely accounted for ^{7}Be outlier values $> 7037\,\mu\mathrm{Bq\,m^{-3}}$ registered at Hornsund in 2010 (Table 1 and Fig. 3).

^{210}Pb ($T_{1/2} = 22.3$ years) is a terrestrial radionuclide belonging to the uranium-radium series. Its presence in the atmosphere is associated with the decay of ^{222}Rn ($T_{1/2} = 3.8$ d), which has previously been exhaled from the Earth's surface into the atmosphere (Gäggeler, 1995). Grossi et al. (2016) noted that, although ^{210}Pb concentrations can increase with altitude and reach high levels in the stratosphere over large continental areas, it primarily accumulates in the troposphere. The majority of ^{210}Pb resides in accumulation-mode aerosol particles, which are mostly removed from the atmosphere by precipitation. Despite differing origins, the behaviour of ^{210}Pb and ^{7}Be in the lower atmosphere was found to be similar for Hornsund, where the annual fluctuation of ^{210}Pb was only slightly offset relative to that of ^{7}Be. Specifically, maximum activity concentrations of ^{210}Pb were identified in the 1st quarter (Fig. 3). These observations corresponded to ^{210}Pb data from Ny-Ålesund, Spitsbergen (Paatero et al., 2003, 2010). Variations of ^{210}Pb in Hornsund were mainly affected by climate patterns and the inflow of continental air masses from northern Asia or Europe. Outlier values of ^{210}Pb exceeding $1091\,\mu\mathrm{Bq\,m^{-3}}$ were noticed in 2008, 2009, 2010, 2015, 2019 and 2020 (Table 1 and Fig. 3), which coincided with reduced sum of precipitation in the respective weeks (Fig. 2d).

An analysis of fission-produced ^{137}Cs ($T_{1/2} = 30.07$ years) revealed a median of $0.26\,\mu\mathrm{Bq\,m^{-3}}$ in ground-level air layers at Hornsund from 2007–2021 (Table 1). A distinct increase in activity concentration, reaching $345\,\mu\mathrm{Bq\,m^{-3}}$, was detected in 2011 (Fig. 3). Elevated ^{137}Cs results – persisting in the atmosphere for approximately 9 weeks – were linked to the FDNPP failure (AMAP, 2015; Burakowska et al., 2021). This accident was identified as the primary source of outlier values (Table 1 and Fig. 3). Additional outliers appeared in 2015 and 2016, but to a far lesser extent (Fig. 3). ^{137}Cs activity concentrations registered at Hornsund generally fell within the background range of approximately $0.05–1.50\,\mu\mathrm{Bq\,m^{-3}}$ established by international air monitoring during 2013–2020 at 17 stations covering most of the Arctic region (Zhang et al., 2022). Interestingly, a clear seasonal pattern was noticed for Yellowknife (62°29′ N, 114°28′ W), where higher levels of ^{137}Cs in summer tightly matched the occurrence of fire plumes at the station location (Zhang et al., 2022). This finding implied that ^{137}Cs deposited worldwide after past nuclear events can be reinjected into the atmosphere on a large scale through combustion and then transported over long distances. In contrast, randomly observed lower ^{137}Cs signals ($< 1\,\mu\mathrm{Bq\,m^{-3}}$) may be due to local resuspension of soil in summer or dust in winter.

3.1.2 Target radioisotopes

Time-series analysis of artificial alpha emitters such as ^{238}Pu, $^{239+240}$Pu, and ^{241}Am suspended in Hornsund air between 2007 and 2021 did not reveal any clear seasonality (Fig. 4). The highest activity concentrations were $6.61\,\mathrm{nBq\,m^{-3}}$ for ^{238}Pu and $15.5\,\mathrm{nBq\,m^{-3}}$ for $^{239+240}$Pu, both in the 3rd quarter of 2015, whereas the maximum for ^{241}Am was $354\,\mathrm{nBq\,m^{-3}}$ in the 1st quarter of 2019 (Fig. 4). Additional peaks were noted in subsequent years: 2017, 2018, 2019, and 2020 for ^{238}Pu; 2010, 2019, 2020, and 2021 for $^{239+240}$Pu; and 2016 for ^{241}Am (Fig. 4). These elevated activity concentrations were classified as outliers (Table 1). Examples of alpha spectra representing outliers of

Table 1. Descriptive statistics for alpha- and gamma-emitters measured in aerosol samples collected at Hornsund between 2007 and 2021 (input dataset available at https://doi.org/10.48733/NO6.25.015, Cwanek, 2025).

	mean	SD	min	*Q1*	median	*Q3*	max	IQR	$Q3 + 3 \times \mathrm{IQR}$
^{7}Be (µBq m^{-3})	2022	1149	188	1177	1853	2642	8378	1465	7037
^{137}Cs (µBq m^{-3})	3.54	28.17	0.07	0.17	0.26	0.45	344.76	0.28	1.28
^{210}Pb (µBq m^{-3})	255	249	10	87	163	338	1649	251	1091
$^{239+240}$Pu (nBq m^{-3})	1.42	2.55	0.23	0.47	0.77	0.97	15.51	0.50	2.48
^{238}Pu (nBq m^{-3})	0.72	1.38	0.02	0.09	0.21	0.59	6.61	0.50	2.09
^{241}Am (nBq m^{-3})	31.4	53.3	2.6	11.3	14.9	33.4	353.6	22.1	99.8

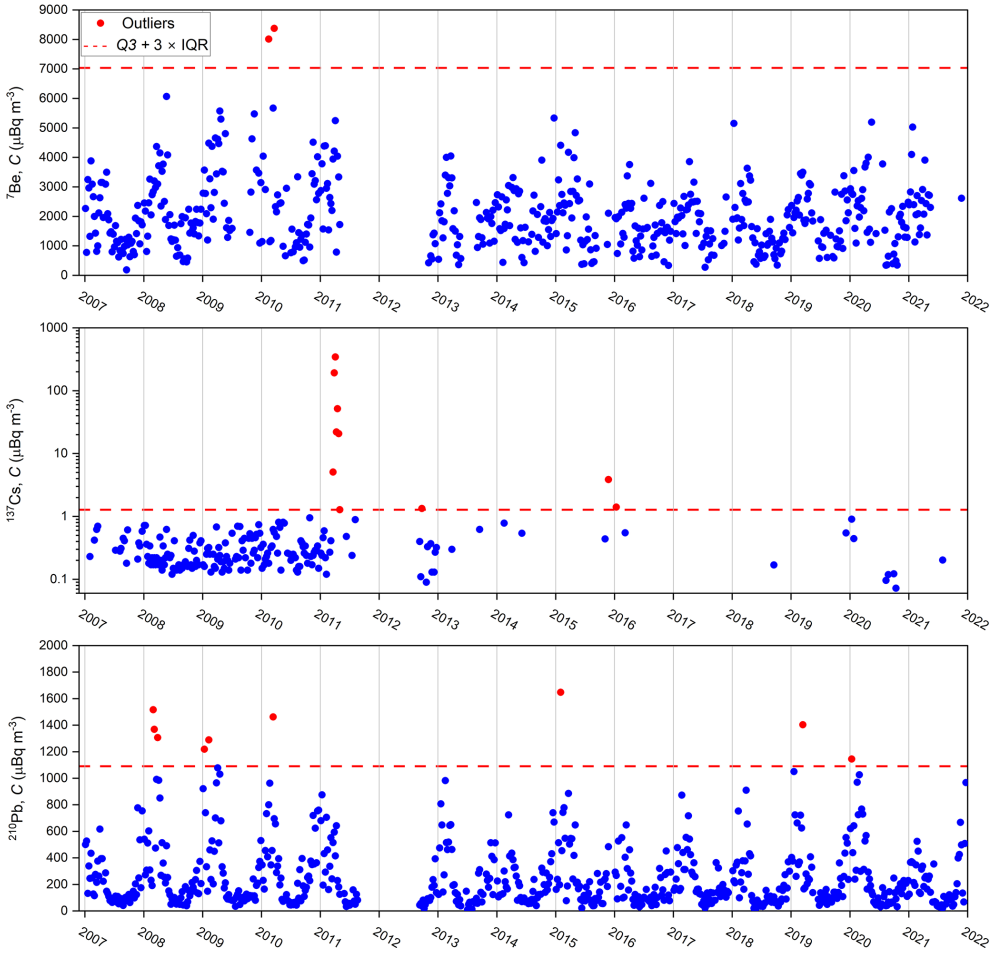

Figure 3. Time series of ^{7}Be, ^{137}Cs, and ^{210}Pb activity concentrations (C) in weekly air filters sampled at Hornsund during 2007–2021. Blue dots indicate non-outlier values, and red dots indicate outlier values.

$^{238,239+240}$Pu in 2015 and ^{241}Am in 2016 are depicted in Fig. S1 in the Supplement. The median values (Table 1) of ^{238}Pu and $^{239+240}$Pu (0.21 nBq m^{-3} and 0.77 nBq m^{-3}, respectively) were approximately two or three orders of magnitude lower than those of ^{241}Am and ^{137}Cs (14.9 nBq m^{-3} and 260 nBq m^{-3}, respectively). The distinct enhancement of ^{137}Cs relative to $^{239+240}$Pu and ^{238}Pu was expected, given that past nuclear events had released at least a tenfold higher activity of ^{137}Cs than $^{239+240}$Pu, ^{241}Am, or ^{238}Pu (UNSCEAR, 1993, 2000a, b). However, a particular challenge arose in explaining why the median of ^{241}Am was notably higher than that of $^{239+240}$Pu. Potential reasons for the observed dynamics of changes and isotopic compositions of artificial actinides in the lower atmosphere of Hornsund for 2007–2021 required further analysis, to be discussed in the next sections.

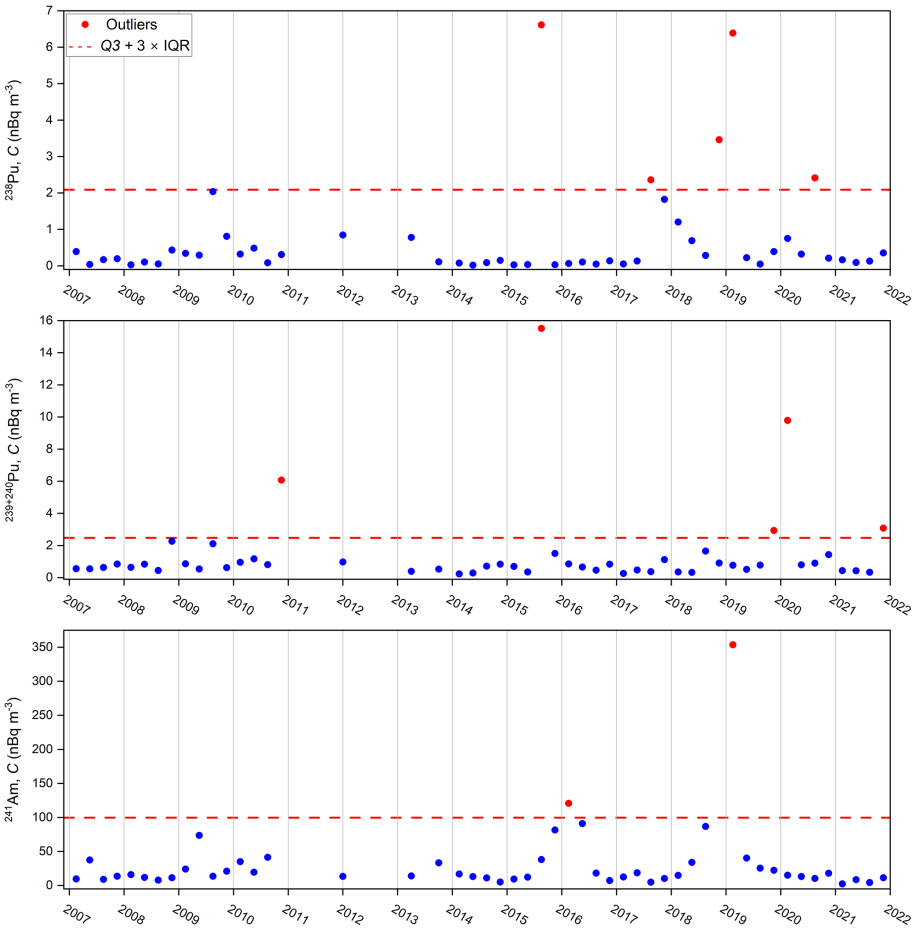

Figure 4. Time series of ^{238}Pu, $^{239+240}$Pu, and ^{241}Am activity concentrations (C) in quarterly air filters sampled at Hornsund during 2007–2021. Blue dots indicate non-outlier values, and red dots indicate outlier values.

Signals of plutonium and americium isotopes were found at various aerosol sampling sites during the 21st century. Nalichowska et al. (2023) studied time series of ^{238}Pu and $^{239+240}$Pu in monthly air filters between 2010 and 2016 in Kraków, Poland (50°04′ N, 19°58′ E). The highest activity concentrations of 1.27 nBq m^{-3} for ^{238}Pu and 13.1 nBq m^{-3} for $^{239+240}$Pu were detected in the 1st and 3rd quarters of 2015, respectively. The mean values of 2.07 nBq m^{-3} for $^{239+240}$Pu and 0.15 nBq m^{-3} for ^{238}Pu in Kraków matched those registered in Hornsund (Table 1). Investigations of monthly aerosol samples collected in Vilnius, Lithuania (54°42′ N, 25°30′ E) showed $^{239+240}$Pu activity concentrations ranging from 0.9–300 nBq m^{-3}, with a mean of 13.4 nBq m^{-3} during 1995–2011. The ^{241}Am results varied between 0.32 and 25 nBq m^{-3}, reaching an average of 4.3 nBq m^{-3} for the shorter period of 2005–2006 (Lujaniene et al., 2012). This implied an order-of-magnitude higher and order-of-magnitude lower levels than those established at Hornsund for $^{239+240}$Pu and ^{241}Am, respectively (Table 1). The Preila air sampling station (55°20′ N, 21°00′ E), situated 300 km from Vilnius, recorded $^{239+240}$Pu activity concentrations of $1-16$ nBq m^{-3}, averaging 6.2 nBq m^{-3} in 1995–1999 (Lujaniene et al., 2012). The disparities between the Preila and Vilnius datasets were attributed to sampling conditions. The Preila station is situated at the Curonian Split on the seashore, where prevailing winds from the Baltic Sea are expected to reduce radionuclide contributions from soil resuspension and the Chernobyl-contaminated zone, compared to the Vilnius station (Lujaniene et al., 2012). Furthermore, a recent study of urban air in Łódź, Poland (51°48′ N, 19°30′ E) identified ^{241}Am signals of 305–4241 nBq m^{-3} in weekly aerosol filters from April to June 2021 (Długosz-Lisiecka and Isajenko, 2024). For the same period, ^{241}Am activity concentrations in surface air at Hornsund declined to several nBq m^{-3}.

Data on ^{238}Pu, $^{239+240}$Pu, and ^{241}Am in the lower atmosphere for northernmost areas during the 21st century are generally unavailable. The primary focus of the research sites mapped in Fig. 1b is on ^{7}Be, ^{133}Xe, ^{137}Cs, and ^{210}Pb (+^{90}Sr, controlled at sites in northern Russia; not marked in Fig. 1b) (AMAP, 2002, 2009, 2015). This investigation, therefore, represents the sole long-term radioactivity-monitoring effort

that has yielded results on artificial actinides in the Arctic atmosphere over the past 2 decades. The previous assessment, encompassing stations proximate to and above the Arctic Circle, was carried out by the NRL from 1957–1962 and continued by the EML SASP between 1963 and 1999 (Larsen et al., 1995). The time series of ^{137}Cs and $^{239+240}$Pu based on data from stations north of 50° N (Kap Tobin, Constable Point, Thule and Nord in Greenland; Barrow in Alaska, USA; Moosonee in Ontario, Canada; Bravo Ocean Station; Charlie Ocean Station) are displayed in Fig. S2. As demonstrated, during the most intense atmospheric nuclear testing (the 1960s), activity concentrations of ^{137}Cs and $^{239+240}$Pu in the air were highest, reaching several thousand $\mu Bq\,m^{-3}$ and $nBq\,m^{-3}$, respectively (Fig. S2). These contamination levels had ceased by the 1980s, once global fallout became negligible, allowing radionuclides from local nuclear emissions and resuspension to dominate in surface air (Chamizo et al., 2010). For instance, the ^{137}Cs peak noted in 1986 was attributed to post-Chernobyl fallout (Fig. S2) (Larsen et al., 1989). The residual activity concentrations of ^{137}Cs and $^{239+240}$Pu observed in the late 1980s and 1990s were consistent with 21st-century data for suspended aerosols at Hornsund (Figs. S2, 3 and 4).

3.2 ^{237}Np incidents

The chemical protocol applied in this study was founded on the premise that neptunium occurs at levels below the detection limits of alpha spectrometry for the majority of environmental samples. According to Kelley et al. (1999), deposited activity of ^{237}Np ($T_{1/2} = 2.144 \times 10^6$ years) is approximately three orders of magnitude lower than that of ^{239}Pu for global fallout. Analyses of three composite samples from Hornsund unexpectedly revealed a distinct ^{237}Np peak that partially overlapped with the ^{242}Pu peak, as shown in Fig. S3. Along with plutonium elution, neptunium is removed from the resin bed; however, no issues are usually experienced during subsequent measurements. This research identified ^{237}Np signals in the 2nd half of 2013, the 1st quarter of 2014, and the 4th quarter of 2018. Overlapping spectral lines were resolved by fitting bigaussian curves, allowing for count integration (Fig. S3). Unfortunately, calculating the activity concentration of ^{237}Np was not feasible because no neptunium tracer was used during the radiochemical procedure. As exemplified in Fig. S4, Pu + Np analytes were successfully separated by an approach that definitively confirmed the presence of ^{237}Np in suspected samples. The ^{237}Np signal in the 4th quarter of 2018 coincided with a ^{238}Pu outlier.

Detection of ^{237}Np was not reported by other researchers in recent aerosol investigations that employed similar radiochemical procedures without separating plutonium and neptunium fractions (Lujaniene et al., 2012; Nalichowska et al., 2023). This prompted us to conduct thorough analyses of the blanks, checking not only the reagents used but also the filter material and equipment in direct contact with the samples examined. The first type of blank comprised only procedural reagents (called "blank"), while the second was a simulated composite sample consisting of 12 cleanly pressed Petrianov filters (called "blank filter"). It was concluded that the presence of radioisotopes in aerosol samples from Hornsund was not due to laboratory contamination or contamination of the spectrometric unit (Table S2). Further quality control was performed on the reference materials IAEA-447 and IAEA-385 to determine the activity concentrations of the target radionuclides ^{238}Pu, $^{239+240}$Pu, and ^{241}Am. The calculated values aligned with the certified values (Table S3).

3.3 Correlation and seasonality evaluation

Spearman's correlation coefficient was selected to minimise the influence of outliers and to account for the non-normal distribution of radioactivity data in Hornsund air (Fig. 5) (Mukaka, 2012; Schober and Schwarte, 2018). The correlation outcomes are summarised in Tables 2–4. The input database used to compute the correlation matrix is provided in Tables S4 and S5.

Mutual correlations were at least moderate or strong for ^{7}Be and ^{210}Pb against air temperature, sum of precipitation, relative humidity, cloudiness, E and NE winds; the latter only for ^{210}Pb (Table 2). Negative monotonic relationships appeared for ^{7}Be and ^{210}Pb versus air temperature, sum of precipitation, relative humidity, and cloudiness, whereas positive monotonic relationships occurred for ^{7}Be and ^{210}Pb with E wind as well as between ^{210}Pb and NE wind. Moreover, ^{7}Be and ^{210}Pb were not affected by the SPM factor (Table 3). These findings corroborated the conclusion concerning the atmospheric transportation and behaviour of ^{7}Be and ^{210}Pb, which were carried into Hornsund by prevailing easterly winds and scavenged by precipitation. Interestingly, quarterly data provided sufficient time resolution to identify correlations between climatic factors and natural radioisotopes. The case of ^{137}Cs seems highly questionable at this point, given that the large number of weekly filters have not shown ^{137}Cs levels above the detection limit since 2013 (Table S5). Artificial radioisotopes exhibited no statistically significant response to climatic conditions, except for $^{239+240}$Pu versus sunshine duration (Table 2). Further evaluation revealed a positive but weak correlation between $^{239+240}$Pu and the SPM parameter (Table 3). Dust concentrations usually peaked in the 4th quarter (Fig. 2c, Table S5), coinciding with enhanced cyclone activity during winter months (Wawrzyniak and Osuch, 2020). Thus, the SPM contribution evidenced a partly local origin for $^{239+240}$Pu, likely due to dust redistribution in winter and minimal soil resuspension in summer. This also explained the weak negative correlation of $^{239+240}$Pu with sunshine duration ($^{239+240}$Pu signals were higher during polar night months than during polar day months).

Strong positive correlations between ^{7}Be and ^{210}Pb were observed annually and in specific quarters (1st, 2nd, and 4th)

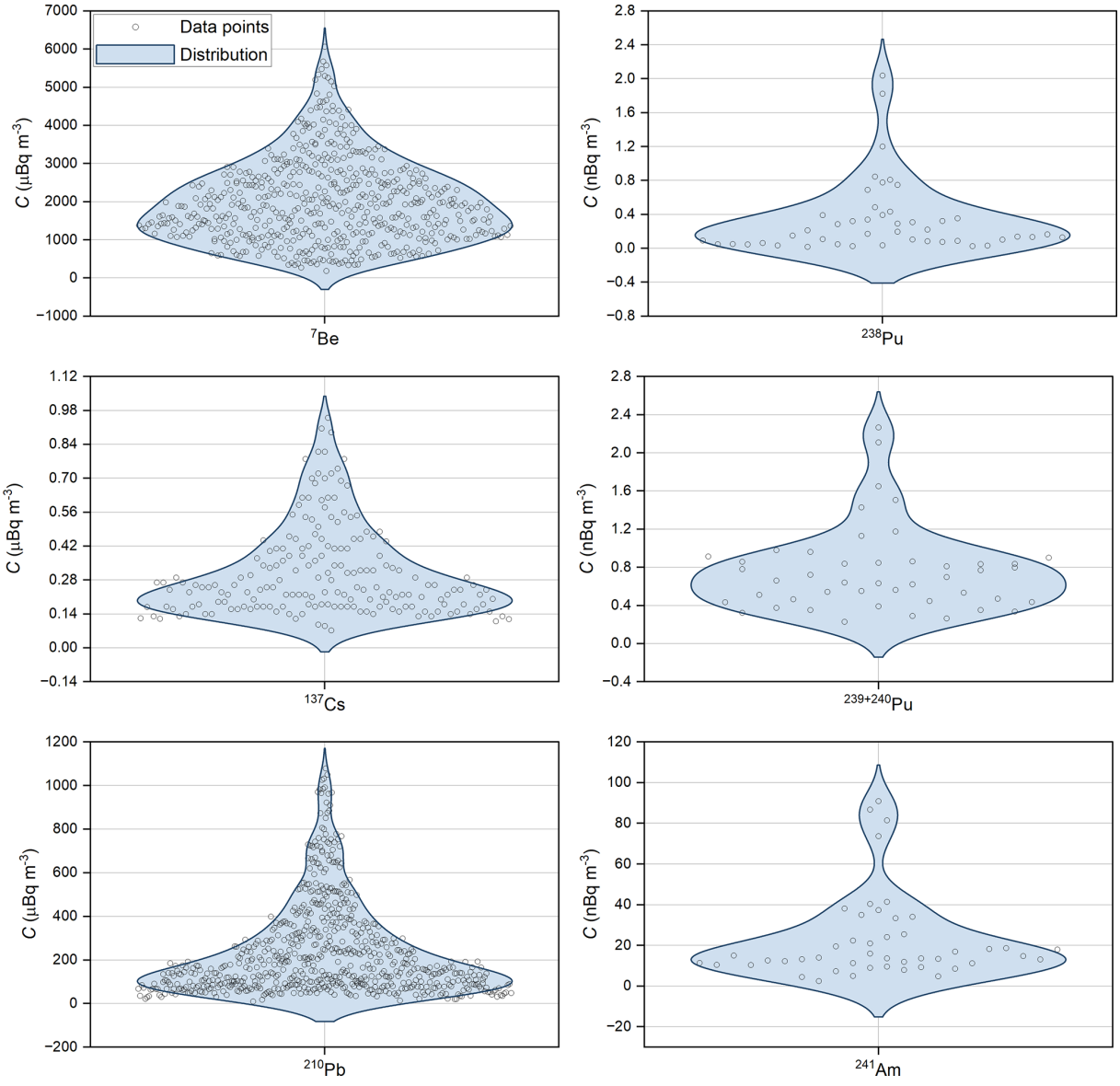

Figure 5. Combined violin and scatter plots for ^{7}Be, ^{137}Cs, ^{210}Pb, ^{238}Pu, $^{239+240}$Pu, and ^{241}Am activity concentrations (C) in weekly or quarterly aerosol samples collected at Hornsund between 2007 and 2021.

(Table 4). Strong correlations were also noted for $^{239+240}$Pu with ^{7}Be, $^{239+240}$Pu with ^{210}Pb, and ^{137}Cs with ^{7}Be in the 1st quarter, as well as between $^{239+240}$Pu and ^{241}Am in the 3rd quarter (Table 4). All of these relationships were positively monotonic, except for ^{137}Cs versus ^{7}Be. It seems that horizontal air-mass movement significantly contributed to transporting $^{239+240}$Pu alongside ^{7}Be and ^{210}Pb during the 1st quarter. The linkage between ^{241}Am and $^{239+240}$Pu in the 3rd quarter might reflect a similar supply pattern, although this was difficult to define. Moreover, a weak positive correlation of $^{239+240}$Pu against ^{238}Pu was found annually (Table 4), suggesting that a small part of ^{238}Pu was likely governed by the natural mechanisms identified for $^{239+240}$Pu. Consistent seasonal fluctuations in the quarterly median values were evident pairwise between ^{7}Be and ^{210}Pb, as well as for $^{239+240}$Pu and ^{238}Pu (Fig. 6). No clear seasonality was noticed for ^{137}Cs and ^{241}Am.

3.4 Potential origin of radioactive contamination

The activity ratios (IR) of artificial actinides were investigated to infer their provenance (Table S7 and Fig. 7), taking into account reference signatures for specific nuclear events provided in Table S6. These ratios are known to vary with reactor type, neutron flux and energy, nuclear fuel burn-up duration, or, for fallout from nuclear detonations, bomb type and yield (Oughton et al., 2001). Typically, ^{238}Pu/$^{239+240}$Pu

Table 2. Mutual correlations between radioisotopes and selected meteorological indicators.

	^{7}Be		^{137}Cs		^{210}Pb		$^{239+240}$Pu		^{238}Pu		^{241}Am	
	R	*p*	*R*	*p*	*R*	*p*	*R*	*p*	*R*	*p*	*R*	*p*
Air temperature	**−0.61***	**0.00**	−0.21	0.25	**−0.90***	**0.00**	−0.03	0.84	−0.16	0.29	−0.02	0.92
Sum of precipitation	**−0.47***	**0.00**	−0.27	0.14	**−0.48***	**0.00**	0.18	0.24	−0.03	0.87	−0.11	0.50
Relative humidity	**−0.41***	**0.00**	−0.29	0.11	**−0.75***	**0.00**	0.10	0.52	−0.22	0.16	0.01	0.97
Cloudiness	**−0.52***	**0.00**	−0.09	0.64	**−0.80***	**0.00**	−0.01	0.97	−0.23	0.14	0.00	0.99
Sunshine duration	0.08	0.58	−0.08	0.67	−0.32*	0.01	−0.38*	0.01	−0.20	0.19	0.23	0.13
Visibility	0.10	0.47	−0.16	0.39	−0.12	0.39	−0.20	0.20	0.08	0.63	0.22	0.15
Air pressure	0.01	0.96	−0.17	0.37	−0.23	0.09	−0.27	0.08	0.01	0.94	0.27	0.08
N	0.00	0.97	0.22	0.22	0.11	0.43	0.12	0.43	−0.14	0.38	–	–
NE	0.26	0.06	0.27	0.14	**0.57***	**0.00**	0.30	0.06	0.29	0.06	−0.14	0.37
E	**0.46***	**0.00**	0.21	0.25	**0.55***	**0.00**	0.25	0.10	0.29	0.06	−0.03	0.83
SE	−0.16	0.25	0.19	0.31	−0.28*	0.03	−0.08	0.60	−0.20	0.20	0.04	0.80
S	−0.35*	0.01	−0.23	0.21	−0.35*	0.01	0.10	0.54	−0.17	0.27	0.11	0.47
SW	−0.08	0.55	−0.15	0.40	−0.13	0.32	−0.13	0.39	−0.17	0.27	−0.11	0.47
W	−0.13	0.33	−0.08	0.68	−0.15	0.27	−0.16	0.31	−0.18	0.26	−0.16	0.31
NW	0.22	0.12	−0.11	0.57	0.18	0.19	−0.13	0.41	−0.13	0.39	0.11	0.49

Statistically significant items ($p \leq 0.05$) are marked with asterisks (*). Moderate and strong correlations ($|R| \geq 0.4$) are highlighted in bold.

Table 3. Mutual correlations between radioisotopes and SPM.

	SPM concentration	
	R	*p*
$^{239+240}$Pu	0.32*	0.04
^{238}Pu	0.23	0.13
^{241}Am	−0.05	0.73
^{7}Be	0.06	0.67
^{137}Cs	0.05	0.77
^{210}Pb	0.23	0.08

Statistically significant items ($p \leq 0.05$) are marked with asterisks (*).

and ^{241}Am/$^{239+240}$Pu ratios in nuclear reactors (NPP) and fuel reprocessing plants (NRP) are about an order of magnitude higher than those for global fallout (GF) or isotopic production grade (PPP) (Table S6).

The ^{238}Pu/$^{239+240}$Pu values ranged from 0.021–8.3, whereas the ^{241}Am/$^{239+240}$Pu values varied from 1.5–460 in Hornsund air (Table S7). Noteworthy, both maxima were observed in the 1st quarter of 2019. The ^{238}Pu/$^{239+240}$Pu ratios exhibited considerable variability throughout 2007–2021, mainly fluctuating within the reference limits of GF (+ SNAP 9A) and Chernobyl fallout (Fig. 7). These results indicated a mixed plutonium origin, influenced by both GF (+ SNAP 9A) and releases from nuclear power plants or nuclear reprocessing plants. Moreover, only one point corresponded to the GF (+ SNAP 9A) level, while several points from 2009–2013 and 2017–2020 displayed ^{238}Pu/$^{239+240}$Pu ratios significantly above the known reference signatures (Fig. 7). The latter issue persisted in the ^{241}Am/$^{239+240}$Pu data, demonstrating an unprecedented enrichment of ^{241}Am relative to established activity ratios for prior nuclear events (Fig. 7 and Table S7).

Radioactive contamination in the Arctic has occurred at two different scales (AMAP, 2002, 2009):

a. widespread contamination associated with global nuclear weapons testing (88 of which took place at the Arctic test site of Novaya Zemlya), releases from Sellafield and Cap de la Hague, and failures at Chernobyl or Fukushima,

b. localised contamination of smaller areas, for instance, from the bomber crash in Thule and from radioactive waste dumped at sea near Novaya Zemlya (e.g., Abrosimov Fjord, Stepovogo Fjord).

The presence of plutonium and americium fallout from nuclear weapon tests has been well documented in the Spitsbergen region, whereas no such influence has been evidenced following the Chernobyl, Fukushima, or Thule accidents (Eriksson et al., 2004; Gwynn et al., 2004; Łokas et al., 2013, 2017b). Nevertheless, elevated ^{238}Pu/$^{239+240}$Pu ratios for cryoconite collected in 2011 and 2014 from Hans Glacier on the northern coast of Hornsund indicated a likely contribution from plutonium sources beyond global fallout (Łokas et al., 2016). The highest recorded value of ^{238}Pu/$^{239+240}$Pu was 0.118 ± 0.017. Additionally, the ^{241}Am/$^{239+240}$Pu ratios were determined for soils and lake sediments in central Spitsbergen, as well as for proglacial and tundra soils from southwestern Spitsbergen, collected in 2005 and 2007 (Łokas et al., 2017b, a). The results varied from 0.18–1.05 in soils and sediments, and from 0.18–0.88 in proglacial soils, with maximum values well above the GF level. Although

Table 4. Total and seasonal cross-correlations among the examined radionuclides ^{7}Be, ^{210}Pb, ^{137}Cs, ^{238}Pu, $^{239+240}$Pu, and ^{241}Am.

total	^{238}Pu		^{241}Am		^{7}Be		^{137}Cs		^{210}Pb	
	R	*p*	*R*	*p*	*R*	*p*	*R*	*p*	*R*	*p*
$^{239+240}$Pu	0.33*	0.04	0.20	0.21	−0.21	0.19	−0.19	0.41	−0.08	0.63
^{238}Pu	1.00		0.05	0.76	0.13	0.42	0.10	0.64	0.08	0.59
^{241}Am			1.00		−0.01	0.95	0.05	0.84	0.05	0.71
^{7}Be					1.00		0.20	0.30	**0.78***	**0.00**
^{137}Cs							1.00		0.25	0.17
1st quarter	^{238}Pu		^{241}Am		^{7}Be		^{137}Cs		^{210}Pb	
	R	*p*	*R*	*p*	*R*	*p*	*R*	*p*	*R*	*p*
$^{239+240}$Pu	0.01	0.99	0.32	0.41	**0.62***	**0.04**	−0.60	0.21	**0.72***	**0.01**
^{238}Pu	1.00		0.16	0.65	0.06	0.85	0.14	0.76	0.07	0.83
^{241}Am			1.00		0.39	0.26	−0.37	0.47	0.39	0.26
^{7}Be					1.00		**−0.78***	**0.01**	**0.56***	**0.04**
^{137}Cs							1.00		−0.29	0.44
2nd quarter	^{238}Pu		^{241}Am		^{7}Be		^{137}Cs		^{210}Pb	
	R	*p*	*R*	*p*	*R*	*p*	*R*	*p*	*R*	*p*
$^{239+240}$Pu	0.37	0.24	0.14	0.66	0.22	0.50	−0.20	0.80	−0.08	0.81
^{238}Pu	1.00		0.29	0.37	−0.01	0.97	−0.40	0.60	−0.19	0.56
^{241}Am			1.00		−0.39	0.21	−0.40	0.60	−0.17	0.60
^{7}Be					1.00		−0.50	0.39	**0.67***	**0.01**
^{137}Cs							1.00		−0.60	0.28
3rd quarter	^{238}Pu		^{241}Am		^{7}Be		^{137}Cs		^{210}Pb	
	R	*p*	*R*	*p*	*R*	*p*	*R*	*p*	*R*	*p*
$^{239+240}$Pu	0.47	0.21	**0.74***	**0.01**	0.37	0.29	0.07	0.88	0.25	0.47
^{238}Pu	1.00		−0.05	0.9	−0.07	0.87	0.37	0.47	−0.32	0.41
^{241}Am			1.00		0.22	0.52	−0.04	0.94	0.52	0.08
^{7}Be					1.00		0.43	0.34	0.45	0.14
^{137}Cs							1.00		0.20	0.58
4th quarter	^{238}Pu		^{241}Am		^{7}Be		^{137}Cs		^{210}Pb	
	R	*p*	*R*	*p*	*R*	*p*	*R*	*p*	*R*	*p*
$^{239+240}$Pu	−0.05	0.91	0.29	0.49	−0.28	0.46	−0.10	0.87	−0.60	0.09
^{238}Pu	1.00		0.01	0.99	0.53	0.10	−0.21	0.64	−0.21	0.54
^{241}Am			1.00		−0.09	0.80	0.66	0.16	−0.07	0.85
^{7}Be					1.00		0.19	0.65	**0.71***	**0.00**
^{137}Cs							1.00		0.62	0.10

Statistically significant items ($p \leq 0.05$) are marked with asterisks (*). Moderate and strong correlations ($|R \geq 0.4$) are highlighted in bold.

soil, sediment, or cryoconite samples are widely regarded as key environmental matrices in airborne radioactivity investigations, they differ substantially from air filter samples. The former register average contamination accumulated over several years, whereas the latter provide information on airborne pollutants at relatively short intervals (day, week, quarter). Elements of the natural environment exposed to atmospheric fallout over decades are strongly contaminated with a signal from nuclear weapons testing, limiting the ability to detect traces of minor radioactive episodes.

A recent study of air filter samples suggested a mixed origin for plutonium isotopes in Poland and revealed the highest ^{238}Pu/$^{239+240}$Pu ratios of 33.7 ± 3.6 in the 1st quarter of 2000 for Białystok and 1.29 ± 0.25 in the 1st quarter of 2002 for Kraków (Kierepko et al., 2016; Nalichowska et al., 2023). The ^{238}Pu/$^{239+240}$Pu values determined in

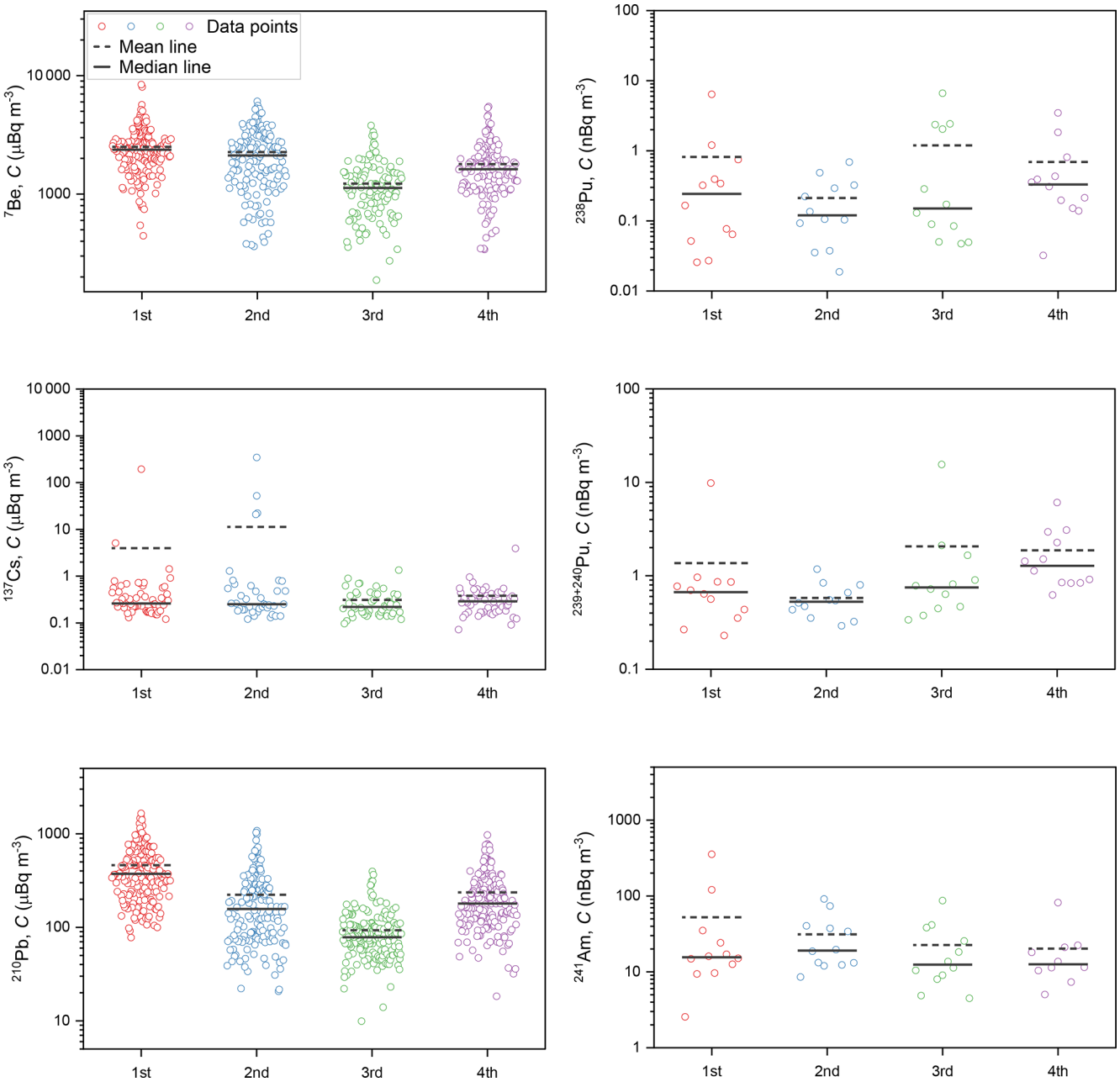

Figure 6. Descriptive statistics and data point distributions in quarters (1st, 2nd, 3rd, 4th) for ^{7}Be, ^{137}Cs, ^{210}Pb, ^{238}Pu, $^{239+240}$Pu, and ^{241}Am activity concentrations (C) in aerosol samples collected at Hornsund between 2007 and 2021.

aerosol samples collected in Vilnius over 2005–2006 varied from 0.028–0.042, whereas ^{241}Am/$^{239+240}$Pu values fell between 0.19 and 0.65, both aligning with the GF (+ SNAP 9A) references. However, a level as high as 1.2 ± 0.1 for ^{238}Pu/$^{239+240}$Pu was detected in Lithuanian air during March–April 2011 (Lujaniene et al., 2012). Results from surface air in Hornsund between 2007 and 2021 showed deviations similar to those of ^{238}Pu/$^{239+240}$Pu in Białystok, Kraków, and Vilnius, but not for ^{241}Am/$^{239+240}$Pu in Vilnius.

The provenance of ^{238}Pu enrichment in the European atmosphere has been widely debated. The following rationale, suggested by researchers, may also offer further insight into Hornsund's situation. Potential sources of plutonium in recently measured aerosol samples are hypothesised to include fuel particles from the Chernobyl or Fukushima accidents and emissions from nuclear facilities (i.e., nuclear power plants, nuclear research centres, or nuclear fuel reprocessing plants) (Wershofen and Arnold, 1998). Hirose and Povinec (2015) proposed that global desert dust events, biomass burn-

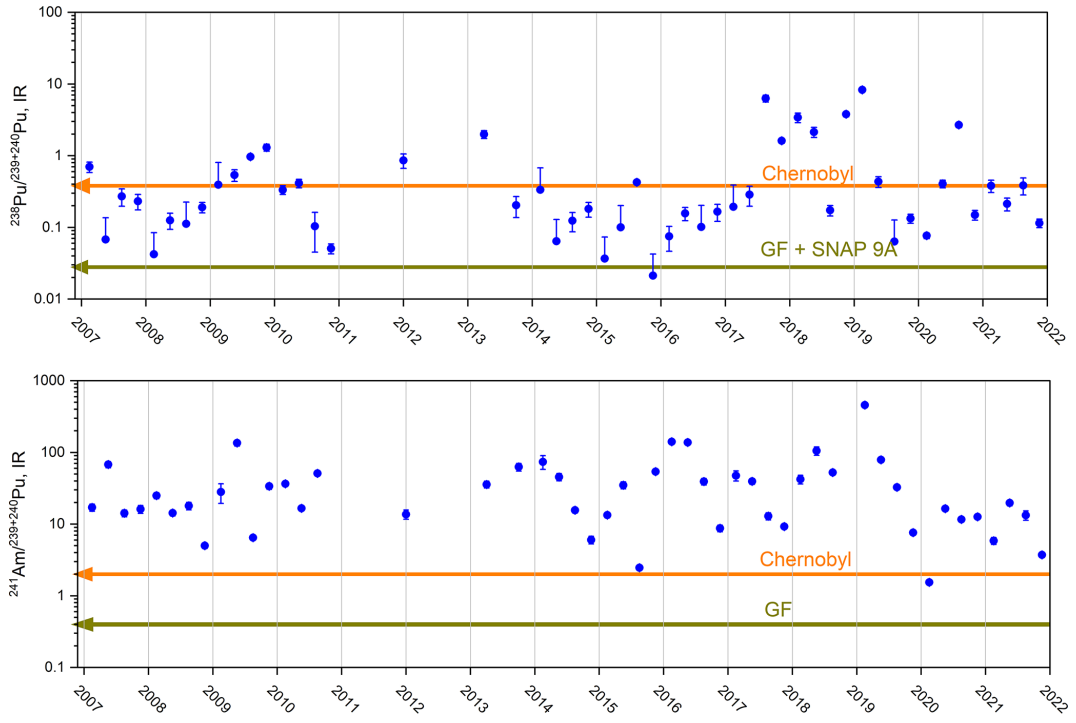

Figure 7. Activity ratios (IR) of ^{238}Pu/$^{239+240}$Pu and ^{241}Am/$^{239+240}$Pu for quarterly aerosol samples collected in Hornsund from 2007–2021 (error bars represent the 1σ level). GF (+ SNAP 9A) and Chernobyl serve as reference values, based on Table S6.

ing, and sea spray are additional likely delivery patterns. Saharan and Asian dust transport has been classified as the most significant mechanism for redistributing aerosols across mid-latitudes. However, Saharan dust displays isotope ratios typical of global fallout (Chamizo et al., 2010). The Chernobyl ecosystem was affected by several major wildfires, notably in 1992, 1999, 2000, 2002–2004, 2006, 2010, 2015, 2016, 2018, and 2020 (Masson et al., 2021). The dispersion of fly ash particles from biomass combustion has been shown to extend over vast distances, both horizontally (up to several thousand kilometres) and vertically (several kilometres), capable of penetrating the tropopause and reaching the lower stratosphere (Hirose and Povinec, 2015). The contribution of plutonium from sea salt to atmospheric plutonium deposition has been found negligible compared to soil's (less than 0.3 %) (Hirose et al., 2003). The maximum calculated input of sea-spray plutonium to the atmosphere did not exceed 0.006 nBq m^{-3}, which is 2–3 orders of magnitude less than that of other plutonium "feeder" mechanisms.

The maximum activity concentration of $^{239+240}$Pu in Hornsund coincided with the highest $^{239+240}$Pu level in Krakow, both noted within the 3rd quarter of 2015. This may indicate a common source behind the $^{239+240}$Pu peaks; however, the corresponding ^{238}Pu/$^{239+240}$Pu signatures differed. Plutonium in Krakow could not be attributed to spent nuclear fuel, while the values of ^{238}Pu/$^{239+240}$Pu and ^{241}Am/$^{239+240}$Pu obtained in Hornsund (0.426 ± 0.017 and 2.46 ± 0.12, respectively) were consistent with Chernobyl reference ratios (Table S7 and Fig. 7). As reported by Evangeliou et al. (2016), about 10.9 TBq of ^{137}Cs, 1.5 TBq of ^{90}Sr, 7.8 GBq of ^{238}Pu, 6.3 GBq of ^{239}Pu, 9.4 GBq of ^{240}Pu, and 29.7 GBq of ^{241}Am were released from two major fires in the Chernobyl Exclusion Zone (CEZ) in April and August 2015. The labile elements escaped more easily from the CEZ, whereas the larger refractory particles were removed more efficiently from the atmosphere, primarily affecting the CEZ and its surroundings. During the summer fire, about 75 % of the labile and 59 % of the refractory radionuclides were exported from the CEZ, with the majority depositing in Belarus and Russia. Although the evolution and fate of the plutonium and americium plume modelled by Evangeliou et al. (2016) suggest no spread to Spitsbergen, scheduled measurements of ^{240}Pu/^{239}Pu mass ratios should ultimately verify the Chernobyl wildfires' impact on the radioactive signals recorded at Hornsund in 2015. The elevated $^{239+240}$Pu activity concentration in Krakow was likely due to intense resuspension associated with a high number of local fires in Poland that could remobilise the global fallout plutonium present in forest litter (Nalichowska et al., 2023).

The above reasoning fails to explain the remarkable enrichment of ^{241}Am between 2007 and 2021, the frequent inputs of ^{238}Pu during 2009–2013 and 2017–2020, or the single injections of ^{237}Np in 2013, 2014, and 2018, all detected at the Hornsund station (Figs. 7 and S3). Correlation assessment indicated that a significant portion of the ^{238}Pu and ^{241}Am must have been introduced into the atmosphere

via non-natural processes (Table 2). Identifying the exclusive nuclear emissions of ^{238}Pu, ^{241}Am, and ^{237}Np is challenging due to the low time resolution of quarterly filters and the scarcity of data on artificial actinides from other stations in the years examined.

^{238}Pu is characterised by sufficient decay heat to power a deep-space satellite or a space probe via a radioisotope thermoelectric generator (RTG). The well-documented source of ^{238}Pu alone is the SNAP 9A high-atmospheric burn-up in 1964 (Krey, 1967). It is doubtful, however, that ^{238}Pu from the SNAP 9A accident has been present in the stratosphere over the last few decades (Hirose and Povinec, 2015). Since the early 2010s, the US government has initiated efforts to restart the production of ^{238}Pu heat-source material for NASA's deep-space missions (Urban-Klaehn et al., 2021; Zillmer et al., 2022). The process involves irradiating a ^{237}Np target with neutrons, converting ^{237}Np into ^{238}Pu. New production relies on reactors at both Oak Ridge National Laboratory (ORNL) and Idaho National Laboratory (INL). These recent nuclear operations have not been associated with reported releases of either ^{238}Pu or ^{237}Np. Radioactive ^{241}Am is commonly used in commercial applications, such as precision measuring devices and smoke detectors. The ^{241}Am activity in various smoke detector models ranges from 7.4–740 kBq, distributed under the class exemption (NUREG-1717, 2001; NUREG/CP-0001, 1978; OECD, 1977). The estimated total number of smoke detectors currently in use for residential purposes in the USA is approximately 100 million, with a total ^{241}Am activity of 12 TBq. The high cost of legal storage for spent devices, coupled with homeowners' lack of awareness, has led to disposal with regular waste or common e-waste without controls. The processing of electrical waste, particularly isotopic smoke detectors, has been postulated to account for the ^{241}Am release in 2021 over central Poland (Długosz-Lisiecka and Isajenko, 2024). Recycling of these devices with general waste, or their combustion at incineration plants, is becoming increasingly popular each year. Importantly, ^{241}Am may also be a generator of ^{237}Np, as the latter is a decay product of ^{241}Am.

Recent nuclear episodes raise new challenges for radioecological research. The presence of ^{106}Ru in European air in autumn 2017 could be linked to an accident at the Mayak nuclear fuel reprocessing plant, involving the separation of large quantities of ^{106}Ru from spent fuel rods. However, alternative explanations include the development of a nuclear engine for powering a small missile or drone (Mietelski and Povinec, 2020). Given that the incident followed an unannounced nuclear operation, the exact scenario for widespread air contamination remains unclear. The Nyonoksa accident in August 2019 (which aligns with official statements about the development of new nuclear-powered missiles in the Russian Federation) may have occurred during preparations to test a nuclear engine driven by either a liquid radioisotope generator ^{42}Ar/^{42}K or a small nuclear reactor (Mietelski and Povinec, 2020). To date, no reports have indicated radioactive leakage into the atmosphere from Nyonoksa. The examples above suggest undeclared nuclear activities. The purpose and types of radioisotopes used are unknown.

A series of transport simulations of nuclear aerosols through the troposphere was performed by the HYSPLIT model, focusing solely on the 1st quarter of 2019. During this period, the highest activity concentration among the examined artificial actinides was found for ^{241}Am. The dispersion of $^{241}AmO_2$ was investigated over a 72 h timeframe, with aerosols predominantly propagating at altitudes up to 1 km. Trajectory modelling was initiated on 1 January and continued until 31 March, as depicted in Figs. 8 and S5. Noteworthy transport pathways from northern Europe and Asia via Novaya Zemlya were observed between January and February (Fig. 8). Nuclear aerosols were carried at low altitudes within the troposphere (often below 100 m), leading to weak dilution and intense deposition. Forward trajectories obtained in early February 2019 indicated substantial material shifts from the Novaya Zemlya region to the aerosol sampling location (Fig. S5). Simulations conducted in early January, late February, and March displayed additional backward trajectories from northern directions (Figs. 8 and S5), which appeared unlikely to transport nuclear aerosols highly enriched in ^{241}Am or other artificial radioisotopes. Reconstructing aerosol propagation during the remaining period – characterised by lower radioisotope activity concentrations than in the 1st quarter of 2019 – was beyond the scope of this paper but is planned to be continued in upcoming scientific exercises.

4 Conclusions

The present study focused on the Arctic troposphere, providing an experimental aerosol database that has improved considerably since 1999. The activity concentrations of ^{238}Pu, $^{239+240}$Pu, and ^{241}Am were determined in the surface air of Hornsund for the years 2007–2021. While the general levels of ^{238}Pu and $^{239+240}$Pu were comparable to recent observations from different sites, ^{241}Am was found to be extraordinarily high, with a maximum of 354 nBq m^{-3} detected in the 1st quarter of 2019. Subsequent analysis of isotopic ratios revealed frequent enrichment of ^{238}Pu relative to $^{239+240}$Pu, inconsistent with previously documented releases. Additionally, unexpected single incidents of ^{237}Np were encountered in 2013, 2014, and 2018.

A multivariate analysis, incorporating data on ^{7}Be, ^{210}Pb, and ^{137}Cs activity concentrations along with a wide range of meteorological factors, was applied to explain the behaviour of artificial actinides in the lower atmosphere. Evaluation of Spearman correlations revealed links between the seasonal trends of $^{239+240}$Pu and natural processes, including local redistribution in winter months and horizontal tropospheric transport of haze layers from remote areas in the 1st quarter. Similar mechanisms controlled a portion of

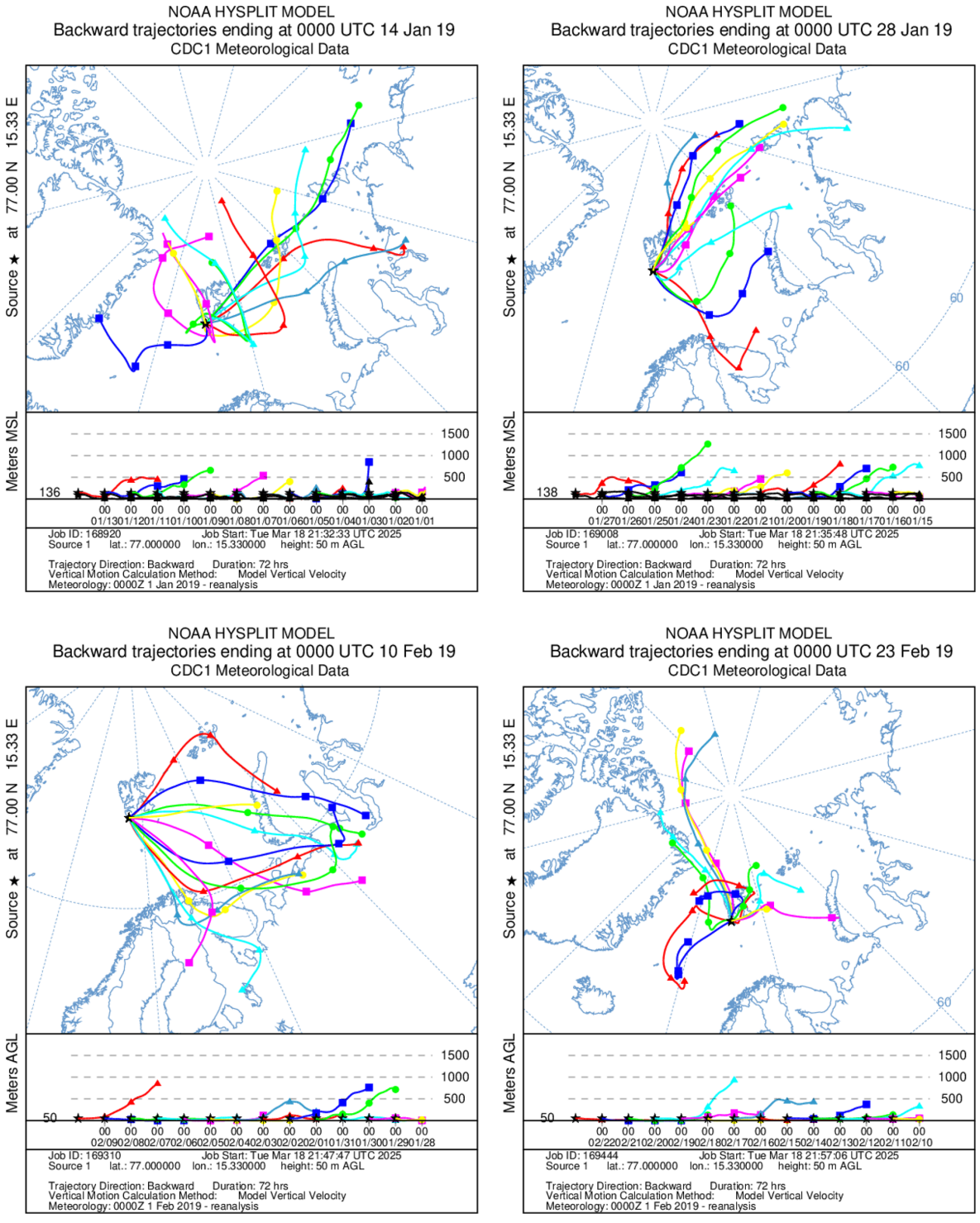

Figure 8. Simulated backward trajectories to the Hornsund study area during the 1st quarter of 2019.

^{238}Pu, but to a lesser extent. Maximum activity concentrations of 6.61 nBq m^{-3} for ^{238}Pu and 15.5 nBq m^{-3} for $^{239+240}$Pu were recorded at Hornsund during the 3rd quarter of 2015. Although these peaks coincided with the resuspension and atmospheric transport of radionuclides triggered by 2015 wildfires near the Chornobyl zone, the plume's arrival in the Arctic remains uncertain.

A majority of the significantly elevated levels of ^{241}Am, ^{238}Pu, and ^{237}Np were not due to natural processes. The average annual doses from exposure to suspended artificial ac-

tinides were negligible, about 1000 times lower than the typical background radiation dose of 2.4 mSv per year. Therefore, the detected contamination did not pose a radiological threat to the Arctic environment. Nevertheless, the ^{241}Am, ^{238}Pu, and ^{237}Np signals were alarming, as their presence could indicate man-made emissions that were overlooked during routine monitoring of gamma emitters in Hornsund air. Trajectory simulations for the 1st quarter of 2019 showed the most prominent transport pathways from northern Europe and Asia via the island of Novaya Zemlya. Nuclear aerosols were carried at low altitudes in the troposphere, leading to weak dilution and intense deposition. The research highlighted the importance of including alpha emitters in routine measurements within radiation situation control programmes.

Data availability. The data are available through the RODBUK Cracow Open Research Data Repository at the Institute of Nuclear Physics, Polish Academy of Sciences, via the following link: https://doi.org/10.48733/NO6.25.015 (Cwanek, 2025).

Supplement. The supplement related to this article is available online at https://doi.org/10.5194/acp-26-5839-2026-supplement.

Author contributions. AC: Writing – original draft, Methodology, Investigation, Formal analysis, Data curation, Conceptualisation, Funding acquisition. AB: Methodology, Investigation, Writing – original draft, Formal analysis. EN: Writing – original draft, Data curation, Formal analysis, Visualisation, Software. MD-L: Writing – original draft, Data curation, Formal analysis, Visualisation. MK: Writing – original draft, Resources, Investigation. TW: Writing – original draft, Data curation. EŁ: Resources, Writing – original draft. MG: Visualisation. GL: Investigation.

Competing interests. The contact author has declared that none of the authors has any competing interests.

Disclaimer. Publisher's note: Copernicus Publications remains neutral with regard to jurisdictional claims made in the text, published maps, institutional affiliations, or any other geographical representation in this paper. The authors bear the ultimate responsibility for providing appropriate place names. Views expressed in the text are those of the authors and do not necessarily reflect the views of the publisher.

Acknowledgements. The authors acknowledge Katarzyna Barnuś, Mikołaj Wielgat, and Michał Palwal for their assistance during laboratory work.

Financial support. The study was conducted at the Stanisław Siedlecki Polish Polar Station in Hornsund, utilising the infrastructure of the Institute of Geophysics, Polish Academy of Sciences. It was funded by the Polish Ministry of Science and Higher Education, with additional support from the Svalbard Integrated Arctic Earth Observing System (SIOS). The National Science Centre of Poland supported the research component focused on alpha-emitter analyses under project no. 2021/43/D/ST10/02049.

Review statement. This paper was edited by Stefano Galmarini and reviewed by two anonymous referees.

References

Aegerter, S., Rama, N. B., and Tamhane, A. S.: ^{7}Be and ^{32}P in ground level air, Tellus, 18, 212–215, https://doi.org/10.3402/tellusa.v18i2-3.9679, 1966.

Alvarado, J. A. C., Steinmann, P., Estier, S., Bochud, F., Haldimann, M., and Froidevaux, P.: Anthropogenic radionuclides in atmospheric air over Switzerland during the last few decades, Nat. Commun., 5, 1–6, https://doi.org/10.1038/ncomms4030, 2014.

AMAP: Radioactivity in the Arctic, Arctic Monitoring and Assessment Programme, Oslo, Norway, ISBN 82-7971-017-5, 2002.

AMAP: Radioactivity in the Arctic, Arctic Monitoring and Assessment Programme, Oslo, Norway, ISBN 978-82-7971-059-2, 2009.

AMAP: Radioactivity in the Arctic, Arctic Monitoring and Assessment Programme, Oslo, Norway, ISBN 978-82-7971-098-1, 2015.

Baré, J., Gheddou, A., and Kalinowski, M. B.: Overview of temporary radioxenon background measurement campaigns conducted for the CTBTO between 2008 and 2018, J. Environ. Radioactiv., 257, https://doi.org/10.1016/j.jenvrad.2022.107053, 2023.

Barrie, L. A., Hoff, R. M., and Daggupaty, S. M.: The influence of mid-latitudinal pollution sources on haze in the Canadian arctic, Atmos. Environ., 15, 1407–1419, https://doi.org/10.1016/0004-6981(81)90347-4, 1981.

Beer, J., McCracken, K., and von Steiger, R.: Cosmogenic Radionuclides – Theory and Applications in the Terrestrial and Space Environments, Springer Berlin Heidelberg, 1689–1699, https://doi.org/10.1017/CBO9781107415324.004, 2019.

Błażej, S. and Mietelski, J. W.: Cosmogenic ^{22}Na, ^{7}Be and terrestrial ^{137}Cs, ^{40}K radionuclides in ground level air samples collected weekly in Kraków (Poland) over years 2003–2006, J. Radioanal. Nucl. Ch., 300, 747–756, https://doi.org/10.1007/s10967-014-3049-6, 2014.

Bossew, P., Gering, F., Petermann, E., Hamburger, T., Katzlberger, C., Hernandez-Ceballos, M. A., De Cort, M., Gorzkiewicz, K., Kierepko, R., and Mietelski, J. W.: An episode of Ru-106 in air over Europe, September–October 2017 – Geographical distribution of inhalation dose over Europe, J. Environ. Radioactiv., 205–206, 79–92, https://doi.org/10.1016/j.jenvrad.2019.05.004, 2019.

Burakowska, A., Kubicki, M., Mysłek-Laurikainen, B., Piotrowski, M., Trzaskowska, H., and Sosnowiec, R.: Concentration of ^{7}Be, ^{210}Pb, ^{40}K, ^{137}Cs, ^{134}Cs radionu-

clides in the ground layer of the atmosphere in the polar (Hornsund, Spitsbergen) and mid-latitudes (Otwock-Świder, Poland) regions, J. Environ. Radioactiv., 240, https://doi.org/10.1016/j.jenvrad.2021.106739, 2021.

Chamizo, E., García-León, M., Enamorado, S. M., Jiménez-Ramos, M. C., and Wacker, L.: Measurement of plutonium isotopes, ^{239}Pu and ^{240}Pu, in air-filter samples from Seville (2001–2002), Atmos. Environ., 44, 1851–1858, https://doi.org/10.1016/j.atmosenv.2010.02.030, 2010.

Coyne, J., Bobrov, D., Bormann, P., Duran, E., Grenard, P., Haralabus, G., Kitov, I., and Starovoit, Y.: CTBTO: Goals, networks, data analysis and data availability, in: New manual of seismological observatory practice 2 (NMSOP-2), Deutsches GeoForschungsZentrum GFZ, 1–41, https://doi.org/10.2312/GFZ.NMSOP-2, 2012.

Currie, L. A.: Limits for Qualitative Detection and Quantitative Determination: Application to Radiochemistry, Anal. Chem., 40, 586–593, https://doi.org/10.1021/ac60259a007, 1968.

Cwanek, A.: Database on air filters collected in the years 2007-2021 in Spitsbergen, Version V3, The Henryk Niewodniczański Institute of Nuclear Physics Polish Academy of Sciences [data set], https://doi.org/10.48733/NO6.25.015, 2025.

Długosz-Lisiecka, M. and Isajenko, K.: Am-241 in the urban air – Monitoring and simulation results, Process. Saf. Environ., 186, 639–644, https://doi.org/10.1016/j.psep.2024.03.124, 2024.

Dueñas, C., Fernández, M. C., Carretero, J., Liger, E., and Cañete, S.: Atmospheric deposition of ^{7}Be at a coastal Mediterranean station, J. Geophys. Res.-Atmos., 106, 34059–34065, https://doi.org/10.1029/2001JD000771, 2001.

Engelbrecht, R. and Schwaiger, M.: State of the art of standard methods used for environmental radioactivity monitoring, Appl. Radiat. Isotopes, 66, 1604–1610, https://doi.org/10.1016/j.apradiso.2008.01.021, 2008.

Eriksson, M., Holm, E., Roos, P., and Dahlgaard, H.: Distribution and flux of ^{238}Pu, ^{239,240}Pu, ^{241}Am, ^{137}Cs and ^{210}Pb to high arctic lakes in the Thule district (Greenland), J. Environ. Radioactiv., 75, 285–299, https://doi.org/10.1016/j.jenvrad.2003.12.007, 2004.

Evangeliou, N., Zibtsev, S., Myroniuk, V., Zhurba, M., Hamburger, T., Stohl, A., Balkanski, Y., Paugam, R., Mousseau, T. A., Møller, A. P., and Kireev, S. I.: Resuspension and atmospheric transport of radionuclides due to wildfires near the Chernobyl Nuclear Power Plant in 2015: An impact assessment, Sci. Rep., 6, https://doi.org/10.1038/srep26062, 2016.

Feely, H. W., Helfer, I. K., Juzdan, Z. R., Klusek, C. S., Larsen, R. J., Leifer, R., Sanderson, C. G., and Dreicer, M.: Fallout in the New York metropolitan area following the Chernobyl accident, J. Environ. Radioactiv., 7, 177–191, https://doi.org/10.1016/0265-931X(88)90006-9, 1988.

Feely, H. W., Larsen, R. J., and Sanderson, C. G.: Factors that cause seasonal variations in Beryllium-7 concentrations in surface air, J. Environ. Radioactiv., 9, 223–249, https://doi.org/10.1016/0265-931X(89)90046-5, 1989.

Furuno, A., Ohmori, R., Tateoka, H., Minakawa, Y., Kurihara, T., Yamamoto, Y., and Tomita, Y.: Assessment of Caesium-137 Detections at CTBTO Radionuclide Monitoring Stations in East Asia and Their Relationship to Asian Dust Dispersion, Pure Appl. Geophys., 182, 5175–5188, https://doi.org/10.1007/s00024-024-03620-y, 2024.

Gäggeler, H. W.: Radioactivity in the Atmosphere, Ract, 70–71, 345–354, https://doi.org/10.1524/ract.1995.7071.s1.345, 1995.

Gorzkiewicz, K., Kierepko, R., Paatero, J., Virkkula, A., and Mietelski, J. W.: Air radioactivity in Marambio Base: The peculiar character of Antarctic Peninsula, J. Environ. Radioactiv., 251–252, 106930, https://doi.org/10.1016/j.jenvrad.2022.106930, 2022.

Grossi, C., Ballester, J., Serrano, I., Galmarini, S., Camacho, A., Curcoll, R., Morguí, J. A., Rodò, X., and Duch, M. A.: Influence of long-range atmospheric transport pathways and climate teleconnection patterns on the variability of surface ^{210}Pb and ^{7}Be concentrations in southwestern Europe, J. Environ. Radioactiv., 165, 103–114, https://doi.org/10.1016/j.jenvrad.2016.09.011, 2016.

Gwynn, J. P., Dowdall, M., Davids, C., Selnæs, Ø. G., and Lind, B.: The radiological environment of Svalbard, Polar Res., 23, 167–180, https://doi.org/10.3402/polar.v23i2.6277, 2004.

Hirose, K. and Povinec, P. P.: Sources of plutonium in the atmosphere and stratosphere–troposphere mixing, Sci. Rep., 5, 1–9, https://doi.org/10.1038/srep15707, 2015.

Hirose, K., Igarashi, Y., Aoyama, M., Kim, C. K., Kim, C. S., and Chang, B. W.: Recent trends of plutonium fallout observed in Japan: Plutonium as a proxy for desertification, J. Environ. Monitor., 5, 302–307, https://doi.org/10.1039/b212560a, 2003.

Hoaglin, D. C.: John W. Tukey and Data Analysis, Stat. Sci., 18, 311–318, https://doi.org/10.1214/ss/1076102418, 2003.

Hoover, M. D. and Maiello, M. L.: Radioactive Air Sampling Methods, CRC Press Taylor & Francis Group, Boca Raton London New York, 1–581, https://doi.org/10.1097/hp.0b013e318217066b, 2010.

ICRP: 1990 Recommendations of the International Commission on Radiological Protection, ICRP Publication 60, Ann. ICRP, 21, ISBN 0-08-041144-4, 1991.

ICRP: The 2007 Recommendations of the International Commission on Radiological Protection, ICRP Publication 103, Ann. ICRP, 37, ISBN 978-0-7020-3048-2, 2007.

IPCC: IPCC Special Report on the Ocean and Cryosphere in a Changing Climate, edited by: Pörtner, H.-O., Roberts, D. C., Masson-Delmotte, V., Zhai, P., Tignor, M., Poloczanska, E., Mintenbeck, K., Alegría, A., Nicolai, M., Okem, A., Petzold, J., Rama, B., and Weyer, N. M., Cambridge University Press, Cambridge, UK and New York, NY, USA, https://doi.org/10.1017/CBO9781139177245.003, 2019.

Kelley, J. M., Bond, L. A., and Beasley, T. M.: Global distribution of Pu isotopes and ^{237}Np, Sci. Total Environ., 237–238, 483–500, https://doi.org/10.1016/S0048-9697(99)00160-6, 1999.

Kierepko, R., Mietelski, J. W., Ustrnul, Z., Anczkiewicz, R., Wershofen, H., Holgye, Z., Kapała, J., and Isajenko, K.: Plutonium isotopes in the atmosphere of Central Europe: Isotopic composition and time evolution vs. circulation factors, Sci. Total Environ., 569–570, 937–947, https://doi.org/10.1016/j.scitotenv.2016.05.222, 2016.

Koo, Y. H., Yang, Y. S., and Song, K. W.: Radioactivity release from the Fukushima accident and its consequences: A review, Prog. Nucl. Energ., 74, 61–70, https://doi.org/10.1016/j.pnucene.2014.02.013, 2014.

Krey, P. W.: Atmospheric burnup of a plutonium-238 generator, Science (1979), 158, 769–771, https://doi.org/10.1126/science.158.3802.769, 1967.

Kulan, A., Aldahan, A., Possnert, G., and Vintersved, I.: Distribution of ^{7}Be in surface air of Europe, Atmos. Environ., 40, 3855–3868, https://doi.org/10.1016/j.atmosenv.2006.02.030, 2006.

Larsen, R. J.: Letter To The Editor: Global Decrease of Beryllium in Surface Air, J. Environ. Radioactiv., 18, 85–87, https://doi.org/10.1080/13518040701205365, 1993.

Larsen, R. J.: Letter To The Editor: Fission Products Detected in Alaska Following the Tomsk-7 Accident, Int. J. Phytoremediation, 23, 205–209, https://doi.org/10.1080/13518040701205365, 1994.

Larsen, R. J., Haagenson, P. L., and Reiss, N. M.: Transport processes associated with the initial elevated concentrations of Chernobyl radioactivity in surface air in the United States, J. Environ. Radioactiv., 10, 1–18, https://doi.org/10.1016/0265-931X(89)90002-7, 1989.

Larsen, R. J., Sanderson, C. G., and Kada, J.: EML Surface Air Sampling Program, 1990–1993 Data, U.S. Department of Energy, New York, https://doi.org/10.2172/188586, 1995.

Lee, H. N. and Feichter, J.: An intercomparison of wet precipitation scavenging schemes and the emission rates of ^{222}Rn for the simulation of global transport and deposition of ^{210}Pb, J. Geophys. Res., 100, https://doi.org/10.1029/95jd01732, 1995.

Łokas, E., Mietelski, J. W., Ketterer, M. E., Kleszcz, K., Wachniew, P., Michalska, S., and Miecznik, M.: Sources and vertical distribution of ^{137}Cs, ^{238}Pu, $^{239+240}$Pu and ^{241}Am in peat profiles from southwest Spitsbergen, Appl. Geochem., 28, 100–108, https://doi.org/10.1016/j.apgeochem.2012.10.027, 2013.

Łokas, E., Zaborska, A., Kolicka, M., Różycki, M., and Zawierucha, K.: Accumulation of atmospheric radionuclides and heavy metals in cryoconite holes on an Arctic glacier, Chemosphere, 160, 162–172, https://doi.org/10.1016/j.chemosphere.2016.06.051, 2016.

Łokas, E., Wachniew, P., Jodłowski, P., and Gąsiorek, M.: Airborne radionuclides in the proglacial environment as indicators of sources and transfers of soil material, J. Environ. Radioactiv., 178–179, 193–202, https://doi.org/10.1016/j.jenvrad.2017.08.018, 2017a.

Łokas, E., Zwoliński, Z., Rachlewicz, G., Gąsiorek, M., Wilkosz, G., and Samolej, K.: Distribution of anthropogenic and naturally occurring radionuclides in soils and lakes of Central Spitsbergen (Arctic), J. Radioanal. Nucl. Ch., 311, 707–717, https://doi.org/10.1007/s10967-016-5085-x, 2017b.

Lujaniene, G., Valiulis, D., Byčenkien, S., Šakalys, J., and Povinec, P. P.: Plutonium isotopes and ^{241}Am in the atmosphere of Lithuania: A comparison of different source terms, Atmos. Environ., 61, 419–427, https://doi.org/10.1016/j.atmosenv.2012.07.046, 2012.

Marsz, A. and Styszyńska, A.: Climate and Climate Change at Hornsund, Svalbard, Gdynia Maritime University, Gdynia, ISBN 9788374211918, 2013.

Masson, O., Piga, D., Gurriaran, R., and D'Amico, D.: Impact of an exceptional Saharan dust outbreak in France: PM_{10} and artificial radionuclides concentrations in air and in dust deposit, Atmos. Environ., 44, 2478–2486, https://doi.org/10.1016/j.atmosenv.2010.03.004, 2010.

Masson, O., Romanenko, O., Saunier, O., Kirieiev, S., Protsak, V., Laptev, G., Voitsekhovych, O., Durand, V., Coppin, F., Steinhauser, G., De Vismes Ott, A., Renaud, P., Didier, D., Boulet, B., Morin, M., Hýža, M., Camps, J., Belyaeva, O., Dalheimer, A., Eleftheriadis, K., Gascó-Leonarte, C., Ioannidou, A., Isajenko, K., Karhunen, T., Kastlander, J., Katzlberger, C., Kierepko, R., Knetsch, G. J., Kónyi, J. K., Mietelski, J. W., Mirsch, M., Møller, B., Nikolić, J. K., Rusconi, R., Samsonov, V., Simion, E., Steinmann, P., Stoulos, S., Suarez-Navarro, J. A., Wershofen, H., Zapata-García, D., and Zorko, B.: Europe-Wide Atmospheric Radionuclide Dispersion by Unprecedented Wildfires in the Chernobyl Exclusion Zone, April 2020, Environ. Sci. Technol., 55, 13834–13848, https://doi.org/10.1021/acs.est.1c03314, 2021.

Mietelski, J. W. and Povinec, P. P.: Environmental radioactivity aspects of recent nuclear accidents associated with undeclared nuclear activities and suggestion for new monitoring strategies, J. Environ. Radioactiv., 214–215, 106151, https://doi.org/10.1016/j.jenvrad.2019.106151, 2020.

Mietelski, J. W., Gaca, P., and Olech, M. A.: Radioactive contamination of lichens and mosses collected in South Shetlands and Antarctic Peninsula, J. Radioanal. Nucl. Ch., 245, 527–537, 2000.

Mietelski, J. W., Kubica, B., Gaca, P., Tomankiewicz, E., Błażej, S., Tuteja-Krysa, M., and Stobiński, M.: ^{238}Pu, $^{239+240}$Pu, ^{241}Am, ^{90}Sr and ^{137}Cs in mountain soil samples from the Tatra National Park (Poland), J. Radioanal. Nucl. Ch., 275, 523–533, https://doi.org/10.1007/s10967-007-7026-1, 2008.

Mukaka, M. M.: Correlation coefficient and its use, Malawi Med. J., 24, 69–71, 2012.

Nalichowska, E., Mietelski, J. W., Kierepko, R., Ustrnul, Z., Gorzkiewicz, K., Brudecki, K., and Kowalska, A.: Plutonium isotopes in the ground air layer in southern Poland (2010–2016): Source terms, seasonal variability and correlations with meteorological conditions, J. Environ. Radioactiv., 264, 107204, https://doi.org/10.1016/j.jenvrad.2023.107204, 2023.

NUREG-1717: Systematic Radiological Assessment of Exemptions for Source and Byproduct Materials, U.S. Nuclear Regulatory Commission, 2001.

NUREG/CP-0001: Radioactivity in Consumer Products, U.S. Nuclear Regulatory Commission, 1978.

OECD: Recommendations for ionization chamber smoke detectors in implementation of radiation protection standards, Nuclear Energy Agency, Organisation for Economic Co-operation and Development, 1977.

Oughton, D., Day, P., and Fifield, K.: Plutonium measurement using accelerator mass spectrometry: Methodology and applications, Radioactiv. Environm., 1, 47–62, https://doi.org/10.1016/S1569-4860(01)80006-1, 2001.

Paatero, J., Hatakka, J., Holmén, K., Eneroth, K., and Viisanen, Y.: Lead-210 concentration in the air at Mt. Zeppelin, Ny-Ålesund, Svalbard, Phys. Chem. Earth, 28, 1175–1180, https://doi.org/10.1016/j.pce.2003.08.050, 2003.

Paatero, J., Buyukay, M., Holmén, K., Hatakka, J., and Viisanen, Y.: Seasonal variation and source areas of airborne lead-210 at Ny-Ålesund in the High Arctic, Polar Res., 29, 345–352, https://doi.org/10.1111/j.1751-8369.2010.00185.x, 2010.

Povinec, P. P., Gera, M., Holý, K., Hirose, K., Lujaniené, G., Nakano, M., Plastino, W., Sýkora, I., Bartok, J., and Gažák, M.: Dispersion of Fukushima radionuclides in the global atmosphere and the ocean, Appl. Radiat. Isotopes, 81, 383–392, https://doi.org/10.1016/j.apradiso.2013.03.058, 2013.

Rahn, K. A.: Relative importances of North America and Eurasia as sources of arctic aerosol, Atmos. Environ., 15, 1447–1455, https://doi.org/10.1016/0004-6981(81)90351-6, 1981.

Rinke, A., Maturilli, M., Graham, R. M., Matthes, H., Handorf, D., Cohen, L., Hudson, S. R., and Moore, J. C.: Extreme cyclone events in the Arctic: Wintertime variability and trends, Environ. Res. Lett., 12, https://doi.org/10.1088/1748-9326/aa7def, 2017.

La Rosa, J. J., Cooper, E. L., Ghods-Esphahani, A., Jansta, V., Makarewicz, M., Shawky, S., and Vajda, N.: Radiochemical methods used by the IAEA's laboratories at Seibersdorf for the determination of ^{90}Sr, ^{144}Ce and Pu radionuclides in environmental samples collected for the International Chernobyl project, J. Environ. Radioactiv., 17, 183–209, https://doi.org/10.1016/0265-931X(92)90025-O, 1992.

La Rosa, J., Gastaud, J., Lagan, L., Lee, S. H., Levy-Palomo, I., Povinec, P. P., and Wyse, E.: Recent developments in the analysis of transuranics (Np, Pu, Am) in seawater, J. Radioanal. Nucl. Ch., 263, 427–436, https://doi.org/10.1007/s10967-005-0072-7, 2005.

Schober, P. and Schwarte, L. A.: Correlation coefficients: Appropriate use and interpretation, Anesth. Analg., 126, 1763–1768, https://doi.org/10.1213/ANE.0000000000002864, 2018.

Stein, A. F., Draxler, R. R., Rolph, G. D., Stunder, B. J. B., Cohen, M. D., and Ngan, F.: NOAA's HYSPLIT atmospheric transport and dispersion modeling system, B. Am. Meteorol. Soc., 96, 2059–2077, https://doi.org/10.1175/BAMS-D-14-00110.1, 2015.

Steinhauser, G., Brandl, A., and Johnson, T. E.: Comparison of the Chernobyl and Fukushima nuclear accidents: A review of the environmental impacts, Sci. Total Environ., 470–471, 800–817, https://doi.org/10.1016/j.scitotenv.2013.10.029, 2014.

UNSCEAR: Ionizing Radiation: Sources and Biological Effects; ANNEX E. Exposures Resulting from Nuclear Explosions. Report to General Assembly, United Nations Scientific Committee on the Effects of Atomic Radiation, New York, ISBN 92-1-142200-0, 1982.

UNSCEAR: Sources and Effects of Ionizing Radiation; ANNEX B. Exposures from Man-made Sources of Radiation, Report to the General Assembly, United Nations, New York, ISBN 92-1-142200-0, 1993.

UNSCEAR: Sources and Effects of Ionizing Radiation; ANNEX C. Exposures to the Public from Man-made Sources of Radiation. Report to the General Assembly, United Nations, New York, ISBN: 92-1-142238-8, 2000a.

UNSCEAR: Sources and Effects of Ionizing Radiation; ANNEX J. Exposure and Effects of Chernobyl Accident. Report to General Assembly, New York, ISBN: 92-1-142238-8, 2000b.

Urban-Klaehn, J., Miller, D., Gross, B. J., Tyler, C. R., and Dwight, C. C.: Initial phase of Pu-238 production in Idaho National Laboratory, Appl. Radiat. Isotopes, 169, https://doi.org/10.1016/j.apradiso.2020.109517, 2021.

Wawrzyniak, T. and Osuch, M.: A 40-year High Arctic climatological dataset of the Polish Polar Station Hornsund (SW Spitsbergen, Svalbard), Earth Syst. Sci. Data, 12, 805–815, https://doi.org/10.5194/essd-12-805-2020, 2020.

Wershofen, H. and Arnold, D.: Radionuclides in Ground-level Air in Braunschweig – Report of the PTB Trace Survey Station Physikalisch-Technische Bundesanstalt, ISBN: 3-86509-431-7, 1998.

Zhang, W., Paatero, J., Leppänen, A. P., Møller, B., Jensen, L. K., Gudnason, K., Sofiev, M., Anderson, P., Sickel, M., Burakowska, A., Kubicki, M., and Anderson, A.: Evaluation of ^{137}Cs, ^{133}Xe and ^{3}H activity concentrations monitored in the Arctic atmosphere, J. Environ. Radioactiv., 253–254, https://doi.org/10.1016/j.jenvrad.2022.107013, 2022.

Zillmer, A., Green, W., Tyler, C., Gross, B., Rosvall, E., Fradeneck, A., Fishler, J., Reeder, D., Marlow, R., Urban-Klaehn, J., Reichenberger, M., Hill, M., and Howard, R.: Recent ^{238}Pu Production Activities at Idaho National Laboratory, Nucl. Technol., 208, S1–S10, https://doi.org/10.1080/00295450.2022.2105774, 2022.